Computers and Structures 236 (2020) 106266

Contents lists available at ScienceDirect

Computers and Structures

journal homepage: www.elsevier.com/locate/compstruc

Minimum energy adaptive structures – All-In-One problem formulation

Yafeng Wang, Gennaro Senatore *

Applied Computing and Mechanics Laboratory (IMAC), School of Architecture, Civil and Environmental Engineering (ENAC), Swiss Federal Institute of Technology (EPFL), CH-1015 Lausanne, Switzerland

ARTICLE INFO

Article history:
Received 14 November 2019
Accepted 13 April 2020
Available online 27 May 2020

Keywords:
Adaptive structures
Minimum whole-life energy
Mixed integer nonlinear programming
Structural optimization
Active structural control

ABSTRACT

This paper presents a new All-In-One (AIO) implementation of an existing formulation to design adaptive structures through Total Energy Optimization (TEO). The method implemented in previous work is a nested optimization process, here named TEO-Nested. Numerical simulations and experimental testing have shown that the TEO-Nested method produces structures that embody and use significantly lower energy compared to passive designs. However, TEO-Nested does not guarantee solution optimality. The formulation presented in this paper is an AIO optimization based on Mixed Integer Nonlinear Programming (MINLP), here named TEO-MINLP. Element cross-section areas, internal forces, nodal displacements and control commands are treated as continuous variables while the actuator positions as binary variables. Stress and displacement limits are included in the optimization constraints. Case studies of reticular structures are employed to benchmark the solutions with those produced by the TEO-Nested method. Results have shown that both formulations produce similar solutions which are only marginally different in energy terms thus proving that the TEO-Nested method tends to converge to optimal (local) solutions. However, the computation time required by TEO-Nested is only a fraction of that required by TEO-MINLP, which makes the former more suitable for structures of complex layout that are made of many elements.

1. Introduction

Adaptive structures are structural systems which have the ability to counteract actively the external loads through redirection of the internal load path (element forces) and controlled changes of the external geometry. Different to passive structural systems, adaptive structures are equipped with sensors and actuators to be controlled during service. In civil engineering, active control has been mostly implemented for vibration suppression of structures under extreme loading events [1–3]. Different systems including active bracings and columns for buildings and active cable-tendons for bridges have been studied [4–7,45]. Shape control has been investigated to reduce the static as well as the dynamic response of tensegrity structures [8–12], to improve airplane maneuverability through morphing wings [13–15] as well as for the control of direct daylight in buildings [16]. Design methods for adaptive structures generally aim to minimize material mass or control effort or a combination of both [17–20,21,46,47]. In most of these strategies, the structure and the actuation system are optimized separately [23–26,48,49]. However, since the actuator location has a significant influence on material and energetic impacts, simultaneous synthesis of the structural and actuation system is key for the design of an adaptive structure.

Senatore et al. [27,27] presented an All-In-One (AIO) formulation to design adaptive structures through Total Energy Optimization (TEO). The formulation has been implemented for reticular structures equipped with linear actuators. The objective is to minimize the whole-life energy (i.e. total energy) which is made of an embodied part in the material and an operational part for control. Minimization of the whole-life energy leads to adaptive solutions with a reduced environmental impact with respect to passive structures. Active control is employed to counteract the effect of strong loading so that the design is not governed by peak demands. Through controlled length changes, the actuators modify the internal forces as well as the geometry of the structure to ensure it operates within required limits, e.g. admissible stress in the structural elements and displacement limits for serviceability. The structure is designed to withstand normal loading conditions in a passive state (i.e. the actuators are locked in position) while it is actively controlled at the occurrence of strong loading events. This allows large savings of the energy embodied in the material at the cost of a small amount of operational energy for actuation.

The formulation by Senatore et al. [27], here named TEO-Nested, has been so far implemented as a nested optimization process. The embodied and operational energy depend on structural

* Corresponding author.
E-mail addresses: yafeng.wang@epfl.ch (Y. Wang), gennaro.senatore@epfl.ch (G. Senatore).

https://doi.org/10.1016/j.compstruc.2020.106266
0045-7949/

Nomenclature

$\mathbf{B}$	equilibrium matrix
dim	dimension of the structure (2D or 3D)
ee	material energy intensity factor (MJ/kg)
E	Young's modulus
$E_{embodied}$	energy embodied in the material
$E_{operational}$	operational energy required by the active system during service
E_{total}	whole-life energy
$\mathbf{F}$	element force
$\mathbf{F}^B$	Euler buckling load
$\mathbf{F}^C$	element force controlled through actuation $\mathbf{F}^C = \mathbf{F} + \Delta\mathbf{F}$
$\mathbf{F}^L$	element force under live load
$\mathbf{F}^{L\_C}$	element force under live load controlled through actuation $\mathbf{F}^{L\_C} = \mathbf{F}^L + \Delta\mathbf{F}^L$
$\mathbf{F}^P$	element force under permanent load
$\mathbf{F}^{P\_C}$	element force under permanent load controlled through actuation $\mathbf{F}^{P\_C} = \mathbf{F}^P + \Delta\mathbf{F}^P$
F^S	force at which the element stress equals the admissible value for tension σ^T or compression σ^C
H	live load hours of occurrence
$\underset{\sim}{\mathbf{K}}$	stiffness matrix
$\mathbf{K}$	element stiffness matrix
$\mathbf{L}$	element length
LAT	load activation threshold
MUT	material utilization factor
$\mathbf{n}$	actuator layout
$n^{\text{act}}_{\min}$	minimum number of actuators
$n^{\text{act}}_{\max}$	maximum number of actuators
n^{cdof}	number of controlled degrees of freedom
n^{cs}	number of constrained degrees of freedom (i.e. supports)
n^d	number of samples in the load probability distribution
n^{dof}	number of degrees of freedom
n^e	number of structural elements
n^{fdof}	number of free degrees of freedom
n^n	number of nodes
n^p	number of load cases
$\mathbf{P}$	total external load $\mathbf{P} = \mathbf{P}^{ext} + \mathbf{P}^{act}$
$\mathbf{P}^{act}$	equivalent load caused by actuation (actuator load)
$\mathbf{P}_d$	design load
$\mathbf{P}^{dead}$	dead load
$\mathbf{P}^{ext}$	external load
$\mathbf{P}^{live}$	live load
$\mathbf{P}^P$	permanent load
$\mathbf{P}^{self}$	self-weight load
r	degree of static indeterminacy
$\mathbf{u}$	nodal displacement
$\mathbf{u}^{cdof}$	displacement of controlled degrees of freedom
$\mathbf{u}^L$	displacement under live load
$\mathbf{u}^{L\_C}$	displacement under live load controlled through actuation $\mathbf{u}^{L\_C} = \mathbf{u}^L + \Delta\mathbf{u}^L$
$\mathbf{u}^{L\_C\|cdof}$	controlled displacements under live load (extracted from $\mathbf{u}^{L\_C}$)
$\mathbf{u}^P$	displacement under permanent load
$\mathbf{u}^{P\_C}$	displacement under permanent load controlled through actuation $\mathbf{u}^{P\_C} = \mathbf{u}^P + \Delta\mathbf{u}^P$
$\mathbf{u}^{P\_C\|cdof}$	controlled displacements under permanent load (extracted from $\mathbf{u}^{P\_C}$)
$\mathbf{u}^{SLS0}$	serviceability limit (deflection) under permanent load
$\mathbf{u}^{SLS}$	serviceability limit under live load
$\mathbf{W}^F$	work done by actuators under compatible force $\mathbf{F}$
$\mathbf{W}^{\Delta F}$	work done by actuators under force correction $\Delta\mathbf{F}$
$\mathbf{W}'^{(1)}$	actuation work (auxiliary variable) for the first phase of the adaptation process
$\mathbf{W}'^{(2)}$	actuation work (auxiliary variable) for the second phase of the adaptation process
$\boldsymbol{\alpha}$	element cross-section area
$\alpha_{\min}$	cross-section area lower bound
$\Delta\mathbf{F}^L$	force correction caused by actuator commands $\Delta\mathbf{L}^L$
$\Delta\mathbf{F}^P$	force correction caused by actuator commands $\Delta\mathbf{L}^P$
ΔL_{limit}	maximum actuator length change
$\Delta\mathbf{L}$	actuator commands (i.e. control commands)
$\Delta\mathbf{L}^P$	actuator commands under permanent load
$\Delta\mathbf{L}^L$	actuator commands under live load
$\Delta\mathbf{u}^L$	displacement correction caused by actuator commands $\Delta\mathbf{L}^L$
$\Delta\mathbf{u}^P$	displacement correction caused by actuator commands $\Delta\mathbf{L}^P$
η	actuator mechanical efficiency
μ	mean of normal probability distribution
ρ	material density
σ	standard deviation of normal probability distribution
σ^C	admissible stress in compression
σ^T	admissible stress in tension
ω	actuator working frequency

sizing and actuation layout which are both design variables. The actuator placement optimization is formulated as a relaxation of the binary problem into a continuous linear form through sensitivity analysis. Embodied and operational energy minimization are coordinated through an auxiliary design variable, the Material Utilization factor (*MUT*) and an auxiliary state variable, the Load Activation Threshold (*LAT*). The *MUT* can be thought of as the ratio of demand over capacity defined for the structure as a whole. The *LAT* is the lowest intensity loading event that causes a state of stress and/or displacement to violate a limit state. The higher the *MUT*, the more flexible the structure (light-weight) and thus the lower the *LAT* because actuation might be needed to control forces and displacements caused by loading events of lower intensity with respect to the design load. The *MUT* is the main variable ($0\% < MUT \leq 100\%$) employed in an outer loop which contains embodied and operational energy minimization. For illustration purposes, Fig. 1 shows the plot of embodied, operational and total energy as a function of the *MUT*. Varying the *MUT* allows to move from least-weight structures (*MUT* = 100%) with small embodied energy but large operational energy (low *LAT*) to very stiff structures (e.g. *MUT* < 25%) with large embodied energy but small operational energy (high *LAT*). The optimal adaptive structure (optimal structural sizing and actuator placement) is the configuration of minimum energy.

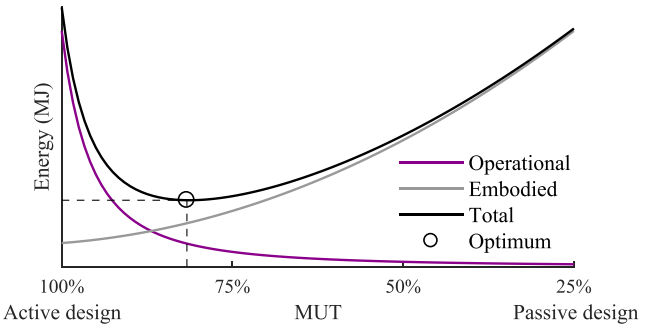

Fig. 1. Embodied, operational and whole-life energy as a function of the Material Utilization factor (MUT) [27].

The TEO-Nested formulation has been applied to the design of reticular structures of complex layout [29,29] and verified experimentally on a large-scale prototype adaptive structure [30]. Results have shown that adaptive structures designed with this method achieve savings up to 70% of the whole-life energy compared to weight-optimized passive structures when the design problem is stiffness governed. The structures produced by this method have not only a lower environmental impact (minimum energy solution) but also a superior structural efficiency because they can be extremely slender and yet they are able to satisfy very tight deflection limits. These characteristics are beneficial for stiffness governed designs including tall buildings, long-spanning bridges and roof systems. The TEO-Nested formulation has also been extended to design structures that adapt to loads through large shape changes accounting for geometric non-linear behavior [32,32].

However, since the TEO-Nested formulation does not carry out a simultaneous optimization of embodied and operational energy, solution optimality is not guaranteed. In addition, the operational energy has been obtained by computing the energy needed for compensation of forces and displacements caused by the external load (one-phase adaptation) but without considering the energy required to control the structure into the configuration prior to actuation after the live load is removed (two-phase adaptation). Although this second phase is often negligible because it usually requires lower actuation forces as the structure returns to the optimal state under permanent load, in some cases it might lead to an inaccurate estimation of the operational energy. One-phase and two-phase adaptation are explained in further detail in Section 2.

This work builds on the TEO-Nested method given in [27] by reformulating the minimum energy design problem into a Mixed Integer Nonlinear Programming (MINLP) problem which can be solved directly to obtain an optimal (local) solution. This new formulation is here named TEO-MINLP. The operational energy is computed considering the full adaptation process (two phases) for both methods. Case studies of simply supported and vertical cantilever truss structures are presented to benchmark the solutions produced by the TEO-MINLP method against the solutions obtained with the TEO-Nested method. This paper is organized as follows. Section 2 gives details of the structural adaptation process that will be simulated. Section 3 gives the All-in-One formulation based on MINLP. Section 4 presents numerical examples. Section 5 and Section 6 conclude the paper.

2. Minimum energy design through structural adaptation

Civil structures are usually capacity designed against the highest demand which is set using statistically predicted worst load cases. However, most load-bearing structures experience loading events that are significantly lower than the design values, which means that the structure is effectively overdesigned for most of the service life. The construction industry is a major contributor to material and energy consumption [34,34]. Most of the embodied impacts for material extraction and fabrication are related to load bearing systems [35]. For these reasons, there is a need of new design methods and technologies to help reduce structures environmental and energetic impacts. Whole-life energy minimization is a new design criterion that was first introduced in [27]. Established design objectives including weight or life-cycle cost minimization do not address explicitly the reduction of structures embodied environmental impacts. If the structure is equipped with an actuation system that controls internal forces and displacements to stay within required limits, the material can be distributed optimally thus saving embodied energy. However, the operational energy required for structural adaptation might be very high if the adaptive structure is not designed to be a minimum configuration in whole-life energy terms. This is a challenging design problem which is non-linear, non-convex and mixed integer [27]. To obtain a minimum energy design, element sizing (element cross-sections), actuator placement as well as actuator commands (length changes) must be determined so that the total energy requirement is kept to a minimum throughout service life.

2.1. Structural adaptation

Fig. 2 illustrates diagrammatically the main steps of the control process as considered in this study. For simplicity of representation, the structure is presented as a generic simply supported beam. However, the configurations considered in this study are pin-jointed structures equipped with linear actuators which are strategically fitted within some of the structural elements (see Section 4). This formulation is implemented within the assumption of small strains and small displacements. The structure is assumed to be subjected to a permanent load (self-weight + dead load) and a randomly varying live load whose probability of occurrence is set as explained in Section 2.3. It is also assumed that the dynamic response of the structure is not controlled by the active system as it was done in [27]. Since dynamic is not considered, seismic design criteria are not included. Because the structure is controlled only against rarely occurring loads, fatigue is not taken as a relevant limit state.

The adaptation process considered in this study is subdivided into the discrete steps (a-f) shown in Fig. 2. The superscript C, which stands for "controlled", denote either element forces or nodal displacements caused by the external load in combination with the effect of actuation. Element forces and nodal displacements caused by the external load without the effect of actuation are also referred to as *compatible*. The forces obtained through actuation are in fact not compatible with the input geometry. Due to geometric compatibility, the effect of actuation is a change of forces and displacements, which is employed to operate the structure within required limits [27]. The forces and displacements obtained through control define an optimal state under each load case. For example, $F^{P\_C} = F^P + \Delta F^P$ and $u^{P\_C} = u^P + \Delta u^P$ is the optimal state under permanent load. The same applies for the live load or other load combination cases.

(a) A first control action is needed under permanent load P^P which causes the element forces F^P and nodal displacements u^P.
(b) In order to eliminate the displacements caused by P^P, the actuators have to change their length by ΔL^P which causes a change of internal forces ΔF^P and displacements Δu^P so that $F^{P\_C} = F^P + \Delta F^P$ and $u^{P\_C} = u^P + \Delta u^P$. This can be thought of as a pre-cambering process so that the structure is kept flat or as close as possible to the input geometry for the general case under permanent load.
(c) When the live load P^L is applied, in this case opposite to P^P, it causes the element forces F^L and nodal displacements u^L which are added to the total element forces and nodal displacements $F^P + \Delta F^P + F^L$ and $u^P + \Delta u^P + u^L$, respectively.
(d) If the total force violates an ultimate limit state (e.g. buckling, material strength limit) or the total displacement exceeds a serviceability limit state, the actuators will apply ΔL^L to cause a change of internal forces ΔF^L and nodal displacements Δu^L. Therefore, the element forces and nodal displacements are $F^P + \Delta F^P + F^L + \Delta F^L$ and $u^P + \Delta u^P + u^L + \Delta u^L$, respectively.
(e) When the live load is removed, the element forces F^L and nodal displacements u^L will also disappear. The total element forces and nodal displacements become $F^P + \Delta F^P + \Delta F^L$ and $u^P + \Delta u^P + \Delta u^L$, respectively.

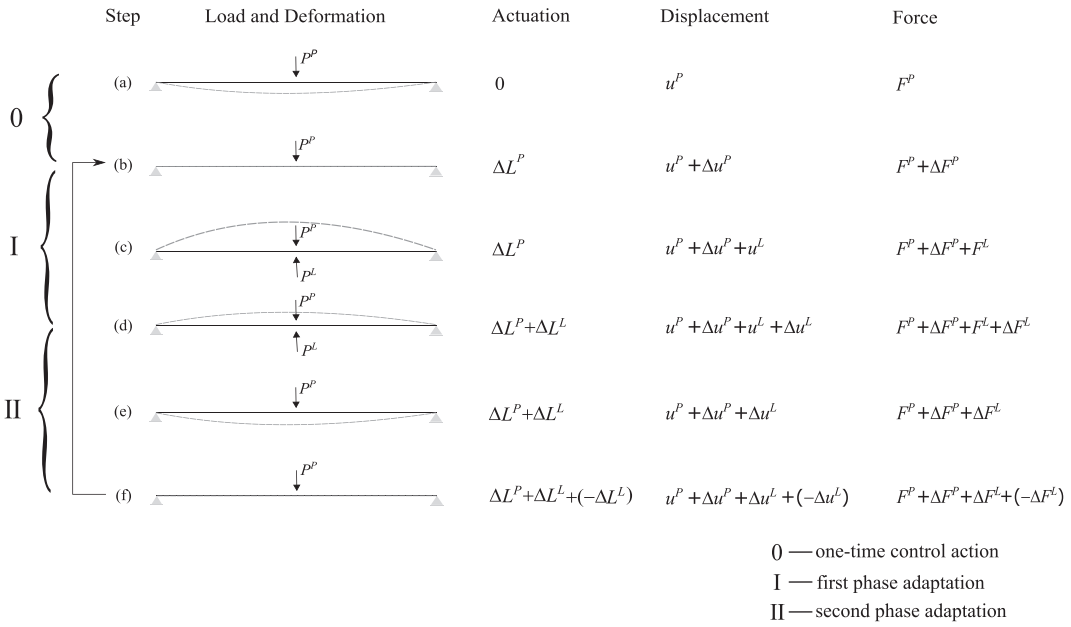

Fig. 2. Load adaptation process.

(f) Although the live load has been removed, the effect of ΔL^L (step d) is still present. Therefore, an opposite change of length $-\Delta L^L$ is applied to remove ΔF^L and Δu^L thus allowing the structure to return to the optimal configuration under permanent load.

Step (b) to step (f) is repeated each time a live load is applied to the structure.

2.2. Operational energy computation

The adaptation process illustrated in Fig. 2 is divided into three steps: (a-b), (b-d), and (d-f). In step (a-b) the structure is controlled to eliminate the displacements caused by the permanent load. This task needs only to be carried out once after or during the building of the structure. Compared to the energy required to control the effect of the live load, the energy required for this one-time actuation is negligible [27]. Steps (b-d) are the first phase of the adaptation process in which the structure is controlled to compensate for the effect of the live load. Steps (d-f) are the second phase of the adaptation process in which the structure is controlled to eliminate the residual effect caused by actuation in the first phase (b-d) and after the live load is removed.

In [27], the operational energy is obtained by accounting only for the first phase (steps b-d) of the adaptation process. In most cases, the energy required by the first phase is much higher than that required in the second phase. This is because, usually, the actuators counteract the effect of the live load in the first phase while during the second phase the actuators release in order to control the structure into the optimal configuration under permanent load (d-f). This is the case for the vertical cantilever structures subject to lateral loading presented in Section 4. However, in other cases, for example when the live load is opposite to the permanent load (such as the case presented in Fig. 2), the situation is inverted. The first phase can be thought of as a relaxation because the total load is actually lower than the permanent load (step b-d) while the second phase requires most of the energy to control the structure into the optimal configuration under permanent load (d-f). This is the case of the simply supported trusses presented in Section 4. For this reason, in this work a two-phase adaptation process is adopted for the computation of the operational energy. In order to compare results obtained by the TEO-MINLP and the TEO-Nested methods, in both formulations the operational energy is computed considering a two-phase adaptation process.

2.3. Live load probability distribution

The computation of the operational energy requires the definition of a probability of occurrence of the loads. For simplicity, all loadings that are not permanent including large events with a small probability of occurrence such as wind storms or unusual crowds are considered as live loads in this work. Following [27], a log-normal distribution is adopted to model the live load probability distribution. Using a log-normal distribution means that the logarithm of the live load event (which is the random variable) is normally distributed. This way it is possible to model a generic random occurrence of the live load whose magnitude is always a positive value. Other probability distributions should be employed to model specific loading events. In order to define the log-normal distribution, the mean μ and the standard deviation σ of the associated normal distribution must be known. For simplicity, the mean μ of the associated normal distribution is set to zero. The design load $\mathbf{P}_d$ is set as the characteristic value which corresponds to the 95th percentile of the associated normal distribution. Since the operational energy is computed during service, the characteristic value is the design load without load factors (SLS load case). Once the characteristic value and the mean are set, the standard deviation of the associated normal distribution is obtained as:

$$\sigma = \frac{\log(\mathbf{P}) - \mu}{\Phi^{-1}(0.95)} \tag{1}$$

where Φ^{-1} is the inverse of the cumulative distribution function of a standard normal distribution.

Fig. 3(a) shows the Cumulative Distribution Function (CDF) of a generic live load, and the dotted line denotes the Load Actuation Threshold (*LAT*). The *LAT* is the lowest level of the load probability distribution that causes a state of stress and/or displacement to violate a limit state [27]. At the left-hand side of the *LAT* are the more frequent loads with low magnitude that the structure can withstand without actuation. At the right side are the rarer loads

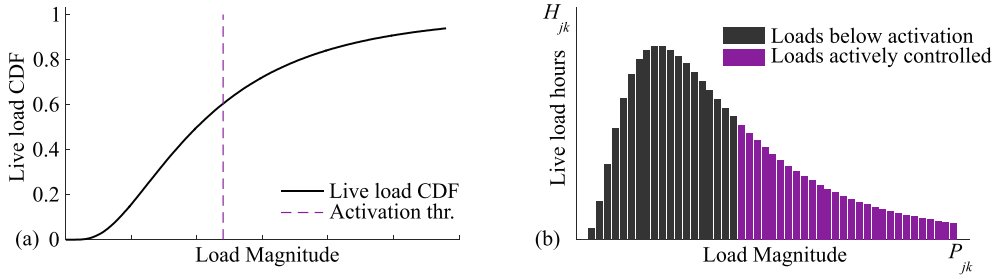

Fig. 3. (a) Live load Cumulative Distribution Function (CDF); (b) live load hours [27]

with higher magnitude which the structure can only withstand through adaptation.

To obtain a discretization of the load probability distribution, given a load case j, all possible values of the load ranging from 0 to the design value $\mathbf{P}_{jd}$ are grouped into n^d bins and the value of the load in the k^{th} bin is denoted by $\mathbf{P}_{jk}$. The number of hours when the live load falls within the k^{th} bin is denoted by H_{jk}. Fig. 3(b) shows the distribution of H_{jk} of a generic live load. The total operational energy during service is the sum of the energy shares that are required to counteract actively loads of magnitude higher than the *LAT*. Note that the *LAT* is not a design variable but rather a state variable. Once the minimum energy configuration is obtained, the *LAT* is computed through analysis.

3. All-In-One Total Energy Optimization formulation

3.1. Reduced model

This section presents the All-In-One Total Energy Optimization (TEO) problem through the reduced formulation given in Table 1 in order to explain the main aspects of the model.

The objective of the optimization is to minimize the whole-life energy of the structure which is the sum of embodied and operational energy as defined in Section 2. This formulation applies to reticular structures equipped with linear actuators. Assume a reticular structure of *dim* dimensions with n^n nodes and n^e elements, and use n^{fdof} to denote the number of degrees of freedom that are not constrained by supports. The main design variables are the element cross-section areas $\alpha \in \mathbb{R}^{n^e \times 1}$, the internal forces $\mathbf{F} \in \mathbb{R}^{n^e \times 1}$ (before control) and $\mathbf{F}^C \in \mathbb{R}^{n^e \times 1}$ (after control), the nodal displacements $\mathbf{u} \in \mathbb{R}^{n^{fdof} \times 1}$ (before control) and $\mathbf{u}^C \in \mathbb{R}^{n^{fdof} \times 1}$ (after control), the actuator layout $\mathbf{n} \in \mathbb{R}^{n^e \times 1}$ which is a vector of binary variables indicating the actuator positions, and the actuator length changes $\Delta\mathbf{L} \in \mathbb{R}^{n^e \times 1}$.

The All-in-One formulation was already given in [27] based on the Integrated Force Method (IFM) [37,37]. However, simulations have shown that that the IFM-based formulation is difficult to solve directly through an AIO optimization scheme because it contains strong nonlinearities. For example, the use of the element flexibility matrix containing $\mathbf{L}/(\mathrm{E}\alpha)$, where $\mathbf{L} \in \mathbb{R}^{n^e \times 1}$ is the element length vector, introduces a non-linearity due to the presence of variable α at the denominator. Therefore, the Dual Integrated Force Method (IFMD) [38] is adopted to reduce the degree of nonlinearity. Note that the governing equations for the IFMD are similar to the stiffness equations with a modification of the load term which allows to incorporate directly the actuator length changes. This variation makes it a convenient method to compute internal forces and nodal displacements resulting from the actuator length changes.

Minimization of the whole-life energy is subjected to four main constraint types: force equilibrium, ultimate limit state (ULS), serviceability limit state (SLS) and actuator layout constraints. Equilibrium of forces is necessary since the internal forces are treated as design variables. For this reason, equilibrium conditions that relate the applied load $\mathbf{P} \in \mathbb{R}^{n^{fdof} \times 1}$ to nodal displacements and element forces through the stiffness matrix $\mathbf{K} \in \mathbb{R}^{n^{fdof} \times n^{fdof}}$ must be satisfied for all cases whether the structure is controlled or not. ULS constrains the element forces (or stresses) to be limited within an admissible value (i.e. material strength limit) for tension σ^T and compression σ^C, which includes local stability constraints $\mathbf{F}^B$ (buckling). SLS is enforced to ensure that the displacements of the controlled degrees of freedom (*cdof*) are kept within required serviceability limit $\mathbf{u}^{SLS}_{\text{limit}}$. The *cdofs* are the degrees of freedom of the nodes that are chosen to be controlled. Actuator layout constraints are implemented to set an upper bound on the maximum number of actuators as well as the maximum actuator length change. Other auxiliary constraints will be formulated to implement the optimization model. Full formulation of the objective function and all constraint equations are given in Section 3.2.

Note that to simplify the notation, element force $\mathbf{F}$, nodal displacement $\mathbf{u}$ and control command $\Delta\mathbf{L}$ are single column vectors by taking only one load case at time. To consider multiple load cases and the load probability distribution discussed in Section 2.3, the formulation is extended for each k^{th} occurrence of the j^{th} load case $\mathbf{P}_{jk}$.

Table 1
TEO-MINLP reduced model.

$\min_{\alpha,\mathbf{F},\mathbf{u},\mathbf{n},\Delta\mathbf{L}}$	$E_{total} = E_{embodied} + E_{operational}$	Objective function
s. t.	$\mathbf{Ku} = \mathbf{P}$	Equilibrium constraints
	$-\sigma^C\boldsymbol{\alpha} \leqslant \mathbf{F}^C \leqslant \sigma^T\boldsymbol{\alpha}$	Ultimate Limit State
	$-\mathbf{F}^B \leqslant \mathbf{F}^C$	
	$-\mathbf{u}^{SLS}_{\text{limit}} \leqslant \mathbf{u}^{C\|cdof} \leqslant \mathbf{u}^{SLS}_{\text{limit}}$	Serviceability Limit State
	$-\Delta L_{\text{limit}}\mathbf{n} \leqslant \Delta\mathbf{L} \leqslant \Delta L_{\text{limit}}\mathbf{n}$	Actuator layout constraints
	–	Auxiliary constraints

3.2. All-In-One Total Energy Optimization full model

3.2.1. Equilibrium conditions

Equilibrium conditions must be satisfied for any load that the structure is designed to withstand whether it is in an active state (controlled through actuation) or in a passive state. By using the IFMD [38], this condition can be expressed as:

$$\mathbf{Ku} = \mathbf{P}, \tag{2}$$

where $\mathbf{K} \in \mathbb{R}^{n^{fdof} \times n^{fdof}}$ is the stiffness matrix, $\mathbf{u} \in \mathbb{R}^{n^{fdof} \times 1}$ is the displacement vector, and $\mathbf{P} \in \mathbb{R}^{n^{fdof} \times 1}$ is the total external load vector which can also include the actuator control commands. Note that Eq. (2) is called "equilibrium" conditions but it also includes geometric compatibility conditions between element deformations and nodal displacements. For reticular structures, the stiffness matrix $\mathbf{K}$ can be expressed as:

$$\mathbf{K} = \mathbf{B}\tilde{\mathbf{K}}\mathbf{B}^{\mathrm{T}}, \tag{3}$$

where $\mathbf{B} \in \mathbb{R}^{n^{fdof} \times n^e}$ is the equilibrium matrix which contains the element direction cosines, and $\tilde{\mathbf{K}} \in \mathbb{R}^{n^e \times n^e}$ is the element stiffness matrix which is diagonal (for truss structures) and whose terms are:

$$\tilde{K}_{ii} = \frac{E_i \alpha_i}{L_i}. \tag{4}$$

The terms E_i, α_i, and L_i are the Young's modulus, cross-section area, and length of the i^{th} element, respectively. The total load $\mathbf{P}$ is expressed as:

$$\mathbf{P} = \mathbf{P}^{ext} + \mathbf{P}^{act}, \tag{5}$$

where $\mathbf{P}^{ext}$ and $\mathbf{P}^{act}$ are the external load and the equivalent load caused by actuation (actuator load for brevity), respectively. $\mathbf{P}^{act}$ is expressed as:

$$\mathbf{P}^{act} = \mathbf{B}\tilde{\mathbf{K}}\Delta\mathbf{L}, \tag{6}$$

where $\Delta\mathbf{L} \in \mathbb{R}^{n^e \times 1}$ is the vector of actuator commands. It is convenient to express the actuator load $\mathbf{P}^{act}$ and length change $\Delta\mathbf{L}$ as vectors of dimensions $\mathbb{R}^{n^e \times 1}$ even if the number of actuators is usually much lower than the number of elements n^e. The length change of the non-active elements is simply set to zero.

Recalling the structural adaptation process explained in Section 2.1, equilibrium conditions must be further divided into two parts depending on whether the live load is applied or not. If only permanent load (dead load $\mathbf{P}^{dead}$ + self-weight $\mathbf{P}^{self}$) (steps a-b in Fig. 2) and the actuator control commands $\Delta\mathbf{L}^P$ are applied, the equilibrium constraints are:

$$\mathbf{K}\mathbf{u}^{P\_C} = \mathbf{P}^P, \tag{7}$$

where

$$\mathbf{P}^P = \mathbf{P}^{dead} + \mathbf{P}^{self} + \mathbf{B}\tilde{\mathbf{K}}\Delta\mathbf{L}^P. \tag{8}$$

Note that $\mathbf{u}^{P\_C}$ in Eq. (7) includes the displacement $\mathbf{u}^P$ caused by the permanent load $\mathbf{P}^{dead}$ + $\mathbf{P}^{self}$ as well as the displacement correction $\Delta\mathbf{u}^P$ caused by $\Delta\mathbf{L}^P$, i.e. $\mathbf{u}^{P\_C} = \mathbf{u}^P + \Delta\mathbf{u}^P$ as shown by step (b) in Fig. 2. The displacement $\mathbf{u}^P$ caused by the permanent load is obtained by removing the actuator load $\mathbf{B}\tilde{\mathbf{K}}\Delta\mathbf{L}^P$ from Eq. (8) and substituting the load in Eq. (7):

$$\mathbf{K}\mathbf{u}^P = \mathbf{P}^{dead} + \mathbf{P}^{self}. \tag{9}$$

$\Delta\mathbf{u}^P$ is then computed as $\Delta\mathbf{u}^P = \mathbf{u}^{P\_C} - \mathbf{u}^P$.

Similarly, equilibrium conditions under the live load $\mathbf{P}^{live}$ are given by:

$$\mathbf{K}\mathbf{u}^{L\_C} = \mathbf{P}^L, \tag{10}$$

where

$$\mathbf{P}^L = \mathbf{P}^{live} + \mathbf{B}\tilde{\mathbf{K}}\Delta\mathbf{L}^L, \tag{11}$$

where $\Delta\mathbf{L}^L$ is the actuator control command to counteract the live load. In Eq. (10) $\mathbf{u}^{L\_C} = \mathbf{u}^L + \Delta\mathbf{u}^L$ as shown by step (d) in Fig. 2. The displacement $\mathbf{u}^L$ caused by the live load is obtained by removing the actuator load $\mathbf{B}\tilde{\mathbf{K}}\Delta\mathbf{L}^L$ in Eq. (11) and substituting the load in Eq. (10):

$$\mathbf{K}\mathbf{u}^L = \mathbf{P}^{live}. \tag{12}$$

$\Delta\mathbf{u}^L$ is then computed as $\Delta\mathbf{u}^L = \mathbf{u}^{L\_C} - \mathbf{u}^L$.

3.2.2. Ultimate Limit State (ULS) constraints

3.2.2.1. Admissible stress and buckling. The controlled element forces are constrained so that the stress does not exceed an admissible limit and compression forces are below the critical buckling load:

$$\begin{cases} -\sigma^C\boldsymbol{\alpha} \leqslant \mathbf{F}^C \leqslant \sigma^T\boldsymbol{\alpha} \\ -\mathbf{F}^B \leqslant \mathbf{F}^C \end{cases}, \tag{13}$$

where σ^C and σ^T are the admissible stress in compression and in tension respectively, $\mathbf{F}^b \in \mathbb{R}^{n^e \times 1}$ is the Euler buckling load vector. For simplicity it is assumed that all elements have a cylindrical hollow section. To reduce optimization complexity, the wall thickness is set proportional to the external diameter. Therefore, $\mathbf{F}^{\boldsymbol{B}}$ is a function of the cross-section area $\boldsymbol{\alpha}$. In addition, element cross-section areas are bounded to be larger than a minimum value $\alpha_{\min}$, which could be used to match commercial availability:

$$\alpha \geqslant \alpha_{\min}. \tag{14}$$

If there is no live load applied to the structure, the controlled element force $\mathbf{F}^C$ is given by:

$$\mathbf{F}^C = \mathbf{F}^{P\_C} = \tilde{\mathbf{K}}\left(\mathbf{B}^{\mathrm{T}}\mathbf{u}^{P\_C} - \Delta\mathbf{L}^P\right). \tag{15}$$

The term that multiplies $\tilde{\mathbf{K}}$ is the elastic deformation of the element which is given by the total deformation $\mathbf{B}^{\mathrm{T}}\mathbf{u}^{P\_C}$ minus the actuator length change $\Delta\mathbf{L}^P$. Note that $\mathbf{F}^{P\_C}$ in Eq. (15) includes both the force $\mathbf{F}^P$ caused by the permanent load and the force correction $\Delta\mathbf{F}^P$ caused by $\Delta\mathbf{L}^P$, i.e. $\mathbf{F}^{P\_C} = \mathbf{F}^P + \Delta\mathbf{F}^P$ as shown by step (b) in Fig. 2. The compatible force (before control) $\mathbf{F}^P$ caused by the permanent load is obtained as:

$$\mathbf{F}^P = \tilde{\mathbf{K}}\mathbf{B}^{\mathrm{T}}\mathbf{u}^P. \tag{16}$$

The force correction $\Delta\mathbf{F}^P$ caused by $\Delta\mathbf{L}^P$ is then computed as $\Delta\mathbf{F}^P = \mathbf{F}^{P\_C} - \mathbf{F}^P$.

If both permanent and live load are applied, $\mathbf{F}^C$ is given by:

$$\mathbf{F}^C = \mathbf{F}^{P\_C} + \mathbf{F}^{L\_C} = \tilde{\mathbf{K}}\left(\mathbf{B}^{\mathrm{T}}\mathbf{u}^{P\_C} - \Delta\mathbf{L}^P\right) + \tilde{\mathbf{K}}\left(\mathbf{B}^{\mathrm{T}}\mathbf{u}^{L\_C} - \Delta\mathbf{L}^L\right). \tag{17}$$

$\mathbf{F}^{L\_C}$ in Eq. (17) includes the force $\mathbf{F}^L$ caused by the live load $\mathbf{P}^{live}$ and the force correction $\Delta\mathbf{F}^L$ caused by $\Delta\mathbf{L}^L$, i.e. $\mathbf{F}^{L\_C} = \mathbf{F}^L + \Delta\mathbf{F}^L$ as shown by step (d) in Fig. 2. The compatible force (before control) $\mathbf{F}^L$ caused by the live load is obtained as:

$$\mathbf{F}^L = \tilde{\mathbf{K}}\mathbf{B}^{\mathrm{T}}\mathbf{u}^L. \tag{18}$$

The force correction $\Delta\mathbf{F}^L$ caused by $\Delta\mathbf{L}^L$ is then computed as $\Delta\mathbf{F}^L = \mathbf{F}^{L\_C} - \mathbf{F}^L$.

3.2.2.2. Fail-safe constraints. A fail-safe constraint enforces the condition that ULS is satisfied even without the contribution of the active system:

$$\begin{cases} -\sigma^C\boldsymbol{\alpha} \leqslant \mathbf{F}^{P\_C} + \mathbf{F}^L \leqslant \sigma^T\boldsymbol{\alpha} \\ -\mathbf{F}^B \leqslant \mathbf{F}^{P\_C} + \mathbf{F}^L \end{cases}, \tag{19}$$

where $\mathbf{F}^{P\_C}$ are the controlled forces under permanent load (one-time control action, see Section 2.1) and $\mathbf{F}^L$ the compatible forces (no control) caused by the live load $\mathbf{P}^L$. In other words, the sum of controlled forces under permanent load and the non-controlled forces under live load must be within required stress and stability limits. This way, in case of a large loading event and concurrent power breakdown and/or control system failure, structure integrity will not be compromised.

3.2.3. Serviceability Limit State constraints

The nodal displacements are constrained to be within prescribed limits:

$$-\mathbf{u}^{\text{limit}} \leqslant \mathbf{u}^{cdof} \leqslant \mathbf{u}^{\text{limit}}, \tag{20}$$

where *cdof* denotes the degrees of freedom to be controlled. If there is no live load applied to the structure, $\mathbf{u}^{cdof} = \mathbf{u}^{P\_C|cdof}$. In this case, the actuator length changes are applied so that the displacements under permanent load are reduced to zero or a very small value as shown by steps (b-d) and steps (d-f) in Fig. 2. This control action can be thought of as a pre-cambering, in this case $\mathbf{u}^{\text{limit}}$ is denoted as $\mathbf{u}^{SLS0}$. If the live load is applied, $\mathbf{u}^{cdof} = \mathbf{u}^{P\_C|cdof} + \mathbf{u}^{L\_C|cdof}$. In this case, $\mathbf{u}^{\text{limit}}$ is assigned as the required serviceability limit which is denoted by $\mathbf{u}^{SLS}$.

3.2.4. Actuator command constraints

The actuator commands are limited so that they do not exceed a prescribed stroke length which otherwise could be impractical. The sign convention for $\Delta\mathbf{L}$ is positive when it is an extension and negative for a contraction. This constraint is formulated as:

$$-\Delta L_{\text{limit}}\mathbf{n} \leqslant \Delta\mathbf{L} \leqslant \Delta L_{\text{limit}}\mathbf{n}, \tag{21}$$

where ΔL_{limit} is the maximum allowed length change, and $\mathbf{n} \in \mathbb{R}^{n^e \times 1}$ is a vector of binary variables $n_i \in \{0, 1\}$ that represents the actuator layout. For clarity, $n_i = 1$ means that i^{th} element is selected to be fitted with a linear actuator. In addition, the number of actuators is constrained by:

$$n^{\text{act}}_{\text{min}} \leqslant \sum_i n_i \leqslant n^{\text{act}}_{\text{max}}, \tag{22}$$

where $n^{\text{act}}_{\text{min}}$ and $n^{\text{act}}_{\text{max}}$ are lower and upper bounds of the number of actuators.

3.2.5. Auxiliary constraints

Following [27], the work W_{ijk} done by the i^{th} actuator for the k^{th} occurrence of the j^{th} load case $\mathbf{P}_{jk}$ is expressed as:

$$W_{ijk} = F_{ijk}\Delta L_{ijk} + \frac{1}{2}\Delta F_{ijk}\Delta L_{ijk}, \tag{23}$$

where F_{ijk} is the compatible element force before control and ΔF_{ijk} is the element force change after the control command ΔL_{ijk} is applied. The products $(F_{ijk}\Delta L_{ijk})$ and $(\frac{1}{2}\Delta F_{ijk}\Delta L_{ijk})$ may be positive or negative. If the terms in $(F_{ijk}, \Delta L_{ijk})$ and/or $(\Delta F_{ijk}, \Delta L_{ijk})$ have the same sign, their product will be positive, for example when an increase of tension is needed for force correction $\Delta F_{ijk} > 0$ through a length extension $\Delta L_{ijk} > 0$ or vice versa for the compression case. In these cases, no work is needed because there is an actual gain of energy which could be harvested. However, since energy harvesting is not considered in this formulation, any energy gain is set to zero in order to compute an upper bound of the operational energy consumption. Therefore, only when the products $(F_{ijk}\Delta L_{ijk})$ and/or $(\frac{1}{2}\Delta F_{ijk}\Delta L_{ijk})$ are negative, their absolute value is added to the operational energy. In order to implement these conditions within the MINLP formulation, two auxiliary variables are introduced, W^F_{ijk} and $W^{\Delta F}_{ijk}$, and a set of auxiliary constraints expressed as:

$$\begin{cases} W^F_{ijk} \leqslant F_{ijk}\Delta L_{ijk} \\ W^{\Delta F}_{ijk} \leqslant \frac{1}{2}\Delta F_{ijk}\Delta L_{ijk} \\ W^F_{ijk} \leqslant 0,\ W^{\Delta}_{ijk} \leqslant 0 \end{cases}. \tag{24}$$

The work W'_{ijk} done by the i^{th} actuator for the k^{th} occurrence of the j^{th} load case $\mathbf{P}_{jk}$ is:

$$W'_{ijk} = -\left(W^F_{ijk} + W^{\Delta F}_{ijk}\right). \tag{25}$$

Note that Eq. (25) is satisfied only at the configuration of minimum energy i.e. when $-\left(W^F_{ijk} + W^{\Delta F}_{ijk}\right)$ reaches the minimum which is ensured because W'_{ijk} is included in the objective function. This way, the operational energy ($E_{operational}$) required for the k^{th} occurrence of the load probability distribution can be computed as:

$$E^k_{operational} = \sum_i \sum_j \frac{W'_{ijk}\omega H_{jk}}{\eta}, \tag{26}$$

where ω is the actuator working frequency expressed in cycles per hour and η the actuator mechanical efficiency. For simplicity, the actuator working frequency is set to the 1st natural frequency, which is likely to dominate the response of most civil structures under dynamic loading [27]. This is a conservative assumption because it means that the actuator will always work at the fundamental frequency even if the load is quasi-static or slow varying. In addition, the TEO-MINLP formulation must be implemented as a single process (see Table 2) i.e. no sub-processes can be included such as the eigenvalue problem to compute the fundamental frequency. Therefore ω is set as the fundamental frequency of the equivalent weight-optimized passive structure. Because the passive structure is always stiffer than the adaptive one, this gives an upper bound on the natural frequency and thus on the operational energy.

3.2.6. Objective function

The optimization objective is minimization of the whole-life energy (E_{total}):

$$E_{total} = E_{embodied} + E_{operational}, \tag{27}$$

where $E_{embodied}$ is the energy embodied in the material and $E_{operational}$ is the total operational energy throughout service life (usually set as 50 years). The embodied energy is:

$$E_{embodied} = \sum_i \alpha_i L_i \rho_i ee_i, \tag{28}$$

where ρ_i is the material density, and ee_i is the energy intensity factor (MJ/kg) [39]. When the structure comprises elements made of a single material, the embodied energy is proportional to the mass through a single scaling factor. However, since the objective is to minimize the structure whole-life energy, the material energy intensity is important even for the case when a single material is adopted.

The operational energy is expressed as:

$$E_{operational} = \sum_i \sum_j \sum_k \frac{\left(W'^{(1)}_{ijk} + W'^{(2)}_{ijk}\right)\omega H_{jk}}{\eta}, \tag{29}$$

where $W'^{(1)}_{ijk}$ and $W'^{(2)}_{ijk}$ are the work shares for the first (steps b-d) and second (steps d-f) control phase respectively done by the i^{th} actuator for the k^{th} occurrence of the j^{th} load case $\mathbf{P}_{jk}$.

3.2.7. TEO-MINLP full model formulation

The TEO-MINLP optimization model is given in Table 2. The vector $\mathbf{X}$ collates the optimization variables: $\mathbf{X} = \left(\begin{matrix}\boldsymbol{\alpha}, \mathbf{F}^{P\_C|SLS}, \mathbf{F}^{L\_C|SLS}, \mathbf{F}^{L|SLS}, \mathbf{F}^{P\_C|ULS}, \mathbf{F}^{L\_C|ULS}, \mathbf{u}^{P\_C|SLS}, \mathbf{u}^{L\_C|SLS}, \mathbf{u}^{L|SLS}, \\ \mathbf{u}^{P\_C|ULS}, \mathbf{u}^{L\_C|ULS}, \Delta\mathbf{L}^{P|SLS}, \Delta\mathbf{L}^{L|SLS}, \Delta\mathbf{L}^{P|ULS}, \Delta\mathbf{L}^{L|ULS}, \mathbf{n}, \mathbf{W}^F, \mathbf{W}^{\Delta F}\end{matrix}\right)$. The superscript *SLS* and *ULS* indicate the design load case without and with load factors, respectively. As explained in Section 2.3, the operational energy is computed during service, hence the objective function and auxiliary constraints contain forces and actuator commands only for the SLS load cases.The factor δ_i in the *Actuator layout constraints* is the load factor for the i^{th} permanent load. This factor is employed to enforce that permanent load cases with the same load factor are controlled with identical actuator commands.

Table 2
TEO-MINLP full model.

$\min_{\mathbf{x}}$	$E_{total} = E_{embodied} + E_{operational}$		Objective function
s. t.	$\mathbf{K}\mathbf{u}^{P\_C\|SLS} = \mathbf{P}^{P\|SLS}$		Equilibrium constraints
	$\mathbf{K}\mathbf{u}_{jk}^{L\_C\|SLS} = \mathbf{P}_{jk}^{L|SLS}$	$\forall j, \forall k$	
	$\mathbf{K}\mathbf{u}_{jk}^{L|SLS} = \mathbf{P}_{jk}^{live}$	$\forall j, \forall k$	
	$\mathbf{K}\mathbf{u}_{j}^{P\_C|ULS} = \mathbf{P}_{j}^{P|ULS}$	$\forall j$	
	$\mathbf{K}\mathbf{u}_{j}^{L\_C|ULS} = \mathbf{P}_{j}^{L|ULS}$	$\forall j$	
	$\mathbf{F}^{P\_C|SLS} = \widetilde{\mathbf{K}}\left(\mathbf{B}^{\mathrm{T}}\mathbf{u}^{P\_C|SLS} - \Delta\mathbf{L}^{P|SLS}\right)$		
	$\mathbf{F}_{jk}^{L\_C|SLS} = \widetilde{\mathbf{K}}\left(\mathbf{B}^{\mathrm{T}}\mathbf{u}_{jk}^{L\_C|SLS} - \Delta\mathbf{L}_{jk}^{L|SLS}\right)$	$\forall j, \forall k$	
	$\mathbf{F}_{jk}^{L|SLS} = \widetilde{\mathbf{K}}\mathbf{B}^{\mathrm{T}}\mathbf{u}_{jk}^{L|SLS}$	$\forall j, \forall k$	
	$\mathbf{F}_{j}^{P\_C|ULS} = \widetilde{\mathbf{K}}\left(\mathbf{B}^{\mathrm{T}}\mathbf{u}_{j}^{P\_C|ULS} - \Delta\mathbf{L}_{j}^{P|ULS}\right)$	$\forall j$	
	$\mathbf{F}_{j}^{L\_C|ULS} = \widetilde{\mathbf{K}}\left(\mathbf{B}^{\mathrm{T}}\mathbf{u}_{j}^{L\_C|ULS} - \Delta\mathbf{L}_{j}^{L|ULS}\right)$	$\forall j$	
	$-\sigma^{C}\boldsymbol{\alpha} \leqslant \mathbf{F}^{P\_C|SLS} \leqslant \sigma^{T}\boldsymbol{\alpha}$		Material strength constraints
	$-\sigma^{C}\boldsymbol{\alpha} \leqslant \mathbf{F}^{P\_C|SLS} + \mathbf{F}_{jk}^{L\_C|SLS} \leqslant \sigma^{T}\boldsymbol{\alpha}$	$\forall j, \forall k$	
	$-\sigma^{C}\boldsymbol{\alpha} \leqslant \mathbf{F}_{j}^{P\_C|ULS} \leqslant \sigma^{T}\boldsymbol{\alpha}$	$\forall j$	
	$-\sigma^{C}\boldsymbol{\alpha} \leqslant \mathbf{F}_{j}^{P\_C|ULS} + \mathbf{F}_{j}^{L\_C|ULS} \leqslant \sigma^{T}\boldsymbol{\alpha}$	$\forall j$	
	$-\mathbf{F}^{B} \leqslant \mathbf{F}^{P\_C|SLS}$		Member buckling constraints
	$-\mathbf{F}^{B} \leqslant \mathbf{F}^{P\_C|SLS} + \mathbf{F}_{jk}^{L\_C|SLS}$	$\forall j, \forall k$	
	$-\mathbf{F}^{B} \leqslant \mathbf{F}_{j}^{P\_C|ULS}$		
	$-\mathbf{F}^{B} \leqslant \mathbf{F}_{j}^{P\_C|ULS} + \mathbf{F}_{j}^{L\_C|ULS}$	$\forall j$	
	$-\mathbf{u}^{SLS0} \leqslant \mathbf{u}^{P\_C|SLS|cdof} \leqslant \mathbf{u}^{SLS0}$		Displacement constraints
	$-\mathbf{u}^{SLS} \leqslant \mathbf{u}^{P\_C|SLS|cdof} + \mathbf{u}_{jk}^{L\_C|SLS|cdof} \leqslant \mathbf{u}^{SLS}$	$\forall j, \forall k$	
	$-\mathbf{u}^{SLS0} \leqslant \mathbf{u}_{j}^{P\_C|ULS|cdof} \leqslant \mathbf{u}^{SLS0}$	$\forall j$	
	$-\mathbf{u}^{SLS} \leqslant \mathbf{u}_{j}^{P\_C|ULS|cdof} + \mathbf{u}_{j}^{L\_C|ULS|cdof} \leqslant \mathbf{u}^{SLS}$	$\forall j$	
	$-\Delta L_{\mathrm{limit}}\mathbf{n} \leqslant \Delta\mathbf{L}^{P|SLS} \leqslant \Delta L_{\mathrm{limit}}\mathbf{n}$		Actuator layout constraints
	$-\Delta L_{\mathrm{limit}}\mathbf{n} \leqslant \Delta\mathbf{L}^{P|SLS} + \Delta\mathbf{L}_{jk}^{L|SLS} \leqslant \Delta L_{\mathrm{limit}}\mathbf{n}$	$\forall j, \forall k$	
	$-\Delta L_{\mathrm{limit}}\mathbf{n} \leqslant \Delta\mathbf{L}_{j}^{P|ULS} \leqslant \Delta L_{\mathrm{limit}}\mathbf{n}$	$\forall j$	
	$-\Delta L_{\mathrm{limit}}\mathbf{n} \leqslant \Delta\mathbf{L}_{j}^{P|ULS} + \Delta\mathbf{L}_{j}^{L|ULS} \leqslant \Delta L_{\mathrm{limit}}\mathbf{n}$	$\forall j$	
	$\Delta\mathbf{L}_{i}^{P|ULS} = \Delta\mathbf{L}_{j}^{P|ULS}$	if $\delta_i = \delta_j$	
	$n_{\min} \leqslant \sum_i n_i \leqslant n_{\max}$		
	$W_{ijk}^{F(1)} \leqslant \left(F_{i}^{P\_C|SLS} + F_{ijk}^{L|SLS}\right)\Delta L_{ijk}^{SLS}$	$\forall i, \forall j, \forall k$	Auxiliary constraints
	$W_{ijk}^{\Delta F(1)} \leqslant \frac{1}{2}\Delta F_{ijk}^{SLS}\Delta L_{ijk}^{SLS}$	$\forall i, \forall j, \forall k$	
	$W_{ijk}^{F(2)} \leqslant \left(F_{i}^{P\_C|SLS} + \Delta F_{ijk}^{SLS}\right)\left(-\Delta L_{ijk}^{SLS}\right)$	$\forall i, \forall j, \forall k$	
	$W_{ijk}^{\Delta F(2)} \leqslant \frac{1}{2}\left(-\Delta F_{ijk}^{SLS}\right)\left(-\Delta L_{ijk}^{SLS}\right)$	$\forall i, \forall j, \forall k$	
	$W_{ijk}^{F(1)} \leqslant 0$	$\forall i, \forall j, \forall k$	
	$W_{ijk}^{\Delta F(1)} \leqslant 0$	$\forall i, \forall j, \forall k$	
	$W_{ijk}^{F(2)} \leqslant 0$	$\forall i, \forall j, \forall k$	
	$W_{ijk}^{\Delta F(2)} \leqslant 0$	$\forall i, \forall j, \forall k$	
	$\alpha \geqslant \alpha_{\min}$		
	$n_i \in \{0, 1\}$	$\forall i$	

The relationships between the load, force, displacement, and actuation with different superscripts are shown in Table 3 and Fig. 2. For simplicity, *SLS* and *ULS* superscripts are omitted in Table 3 and Fig. 2.

Referring to Table 2, the dimensions of the optimization variables are given in Table 4.

Thus, for a structure with n^e elements and n^{fdof} free degrees of freedom, the total number of optimization variable is:

$$\begin{aligned} n_c^v &= 3n^e + n^{fdof} + n^p n^d\left(7n^e + 2n^{fdof}\right) + n^p\left(4n^e + 2n^{fdof}\right) \\ n_b^v &= n^e \end{aligned} \tag{30}$$

where n^p and n^d are the number of load cases and the number of bins of the discretized load probability distribution, respectively; n_c^v and n_b^v are the number of continuous and binary variables, respectively.

Fail-safe constraints can be incorporated in the optimization model through Eq. (19) so that the sum of the controlled forces under permanent load $\mathbf{F}^{P\_C|ULS}$ and the non-controlled forces under live load $\mathbf{F}^{L|ULS}$ (defined in Eq. (18)) is kept within required stress and stability limits. This involves adding $n^p n^e$ variables for $\mathbf{F}^{L|ULS}$. In addition, to ensure equilibrium and compatibility between $\mathbf{F}^{L|ULS}$ and the compatible displacements under live load $\mathbf{u}^{L|ULS}$(defined in Eq. (18)), an extra constraint must be included $\mathbf{F}_{jk}^{L|ULS} = \widetilde{\mathbf{K}}\mathbf{B}^{\mathrm{T}}\mathbf{u}_{jk}^{L|ULS}$ which involves adding $n^p n^{fdof}$ variables for $\mathbf{u}^{L|ULS}$. Hence, the inclusion of fail-safe constraints in the optimization model requires the addition of $n^p\left(n^e + n^{fdof}\right)$ variables. Compared to the total number of variables given in Eq. (30), the inclusion of fail-safe constraints does not cause a significant increase of optimization variables. However, since the examples studied in this work are stiffness governed design problems, the governing constraint is the serviceability limit on deflections. For this reason, in order to simplify the optimization model, fail-safe constraints have not been included. This way it is assumed that the active system contributes to avoid critical stress conditions under loading. A post analysis will be carried out in Section 3.3.3 to assess whether fail-safe conditions are met.

3.3. TEO-MINLP vs TEO-Nested

3.3.1. Actuator layout optimization

In the TEO-Nested method, embodied energy minimization, actuator layout optimization and operational energy computation are carried out for a set of *MUTs*. The configuration of minimum total energy is then selected as the optimal solution. In the TEO-Nested method, force equilibrium and geometric compatibility are disaggregated. In the embodied energy optimization step, the variables are the element cross-section areas and internal forces. Constraints include force equilibrium, material strength and member buckling but neither geometric compatibility nor deflection limits are taken into account. This means that the optimal forces are not compatible and must be enforced through a controlled change of shape. The actuator layout is obtained as the set of n^{act} elements whose length change is most effective to redirect the compatible forces into the optimal ones and to keep nodal displacements within the required limit for multiple load cases. In the TEO-MINLP formulation, force equilibrium and geometric compatibility are combined. The actuator layout is obtained as a direct result from the minimization of the total energy. For this reason, it is expected that the actuator layout of the solutions produced by the TEO-MINLP and TEO-Nested methods will be different.

3.3.2. Operational energy minimization

In the TEO-Nested formulation given in [27], adaptation is employed to control the element forces into target (optimal) forces and to keep the nodal displacements within required limits. The sum of the energy required for adaptation at each occurrence of the load probability distribution above the *LAT* is the operational energy during service. In the TEO-MINLP formulation, the actuator commands are computed through minimization of the operational energy. For this reason, in order to compare these two formulations, the TEO-Nested method has been reformulated to obtain the actuator commands through operational energy minimization. This new method can be thought of as a reduced form of the TEO-MINLP model presented in Section 3.2. The objective function is the minimization of $E_{operational}$ subject to the same constraints as those defined in Section 3.2.

This is a general optimization model which can be employed to minimize the operational energy if the element cross-section areas and the actuator layout are known. The input for this model are the

Table 3
Relations between load, force, displacement and actuation.

Load	Actuation command	Force caused by actuation	Displacement caused by actuation	Force	Displacement
$\mathbf{P}^{dead}+\mathbf{P}^{self}$	–	–	–	$\mathbf{F}^{P}$	$\mathbf{u}^{P}$
$\mathbf{P}^{live}$	–	–	–	$\mathbf{F}^{L}$	$\mathbf{u}^{L}$
$\mathbf{P}^{P}$	$\Delta\mathbf{L}^{P}$	$\Delta\mathbf{F}^{P}$	$\Delta\mathbf{u}^{P}$	$\mathbf{F}^{P\_C}=\mathbf{F}^{P}+\Delta\mathbf{F}^{P}$	$\mathbf{u}^{P\_C}=\mathbf{u}^{P}+\Delta\mathbf{u}^{P}$
$\mathbf{P}^{L}$	$\Delta\mathbf{L}^{L}$	$\Delta\mathbf{F}^{L}$	$\Delta\mathbf{u}^{L}$	$\mathbf{F}^{L\_C}=\mathbf{F}^{L}+\Delta\mathbf{F}^{L}$	$\mathbf{u}^{L\_C}=\mathbf{u}^{L}+\Delta\mathbf{u}^{L}$

Table 4
Dimensions (D) of optimization variables (V).

	Continuous variable						
V	α	$\mathbf{F}^{P\_C\|SLS}$	$\Delta\mathbf{L}^{P\|SLS}$	$\mathbf{u}^{P\_C\|SLS}$			
D	n^e	n^e	n^e	n^{fdof}			
V	$\mathbf{F}^{L\_C\|SLS}$	$\mathbf{F}^{L\|SLS}$	$\Delta\mathbf{L}^{L\|SLS}$	$\mathbf{W}^{F}$	$\mathbf{W}^{\Delta F}$	$\mathbf{u}^{L\_C\|SLS}$	$\mathbf{u}^{L\|SLS}$
D	$n^e\times n^p\times n^d$	$n^e\times n^p\times n^d$	$n^e\times n^p\times n^d$	$n^e\times n^p\times n^d\times 2$	$n^e\times n^p\times n^d\times 2$	$n^{fdof}\times n^p\times n^d$	$n^{fdof}\times n^p\times n^d$
V	$\mathbf{F}^{P\_C\|ULS}$	$\mathbf{F}^{L\_C\|ULS}$	$\Delta\mathbf{L}^{P\|ULS}$	$\Delta\mathbf{L}^{L\|ULS}$	$\mathbf{u}^{P\_C\|ULS}$	$\mathbf{u}^{L\_C\|ULS}$	
D	$n^e\times n^p$	$n^e\times n^p$	$n^e\times n^p$	$n^e\times n^p$	$n^{fdof}\times n^p$	$n^{fdof}\times n^p$	
	Binary variable						
V	$\mathbf{n}$						
D	n^e						

element cross-section areas ($\boldsymbol{\alpha}$), the actuator layout ($\mathbf{n}$), the controlled state under permanent load which comprises element forces ($\mathbf{F}^{P\_C|SLS}$), nodal displacements ($\mathbf{u}^{P\_C|SLS}$) and actuator commands $\Delta\mathbf{L}^{P|SLS}$as well as the load activation threshold (LAT) As defined in Section 2.3, the LAT is the lowest level of the load probability distribution that causes a state of stress and/or displacement to violate a limit state. The $LAT$is obtained by computing the displacements $\mathbf{u}^{L}_{jk}$ and member forces $\mathbf{F}^{L}_{jk}$ caused by the live load $\mathbf{P}^{live}_{jk}$ throughEq. (12) and Eq. (18) for each bin k of the discretized load probability distribution. Structural adaptation is needed for any $k \geq k^*$, where k^* denotes the index of the load occurrence corresponding to the LAT. The full optimization problem is given in Table 5. The vector $\mathbf{X}$collates the optimization variables: $\mathbf{X}=\left(\Delta\mathbf{L}^{L|SLS},\mathbf{u}^{L\_C|SLS},\mathbf{F}^{L\_C|SLS},\mathbf{W}^{F},\mathbf{W}^{\Delta F}\right)$. Note that $\Delta\mathbf{L}^{L}_{jk}(m)$ denotes the m^{th} entry of the vector $\Delta\mathbf{L}^{L}_{jk}$, and I is a set containing the index of the elements that are not selected as active and whose length change must therefore be set to 0. All other constraint equations have been described in Section 3.2.

3.3.3. Force and shape control with fail-safe constraints

As explained in Section 3.2.7, since the examples studied in this paper are stiffness governed, a simplification of the optimization model is possible by excluding fail-safe constraints. However, once the solution is obtained, an analysis has been carried out to assess whether fail-safe conditions are met. To verify this, a new control process has been formulated through optimization. The optimization model is given in Table 6. The vector $\mathbf{X}$ collates the optimization variables:$\mathbf{X}=\left(\Delta\mathbf{L}^{P|ULS},\Delta\mathbf{L}^{L|ULS},\mathbf{u}^{P\_C|ULS},\mathbf{u}^{L\_C|ULS},\mathbf{F}^{P\_C|ULS},\mathbf{F}^{L\_C|ULS}\right)$. The objective is to obtain the smallest $\Delta\mathbf{L}^{P|ULS}$(one-time control under permanent load) and $\Delta\mathbf{L}^{L|ULS}$ such that the fail-safe constraint given in Eq (19) is satisfied. Note that $\Delta\mathbf{L}^{P|ULS}$ is the actuator command for the one-time control action illustrated in steps (a-b) in Fig. 2. This control action can be thought of as part of the construction process similar to pre-stress. For completeness, also $\Delta\mathbf{L}^{L|ULS}$ is considered so that deflection limits are met under the USL load case but it is not part of the fail-safe constraints. The choice of this objective function makes the optimization model linear which, therefore, can be solved efficiently. In addition, it is preferable to satisfy the fail-safe constraints using small actuator length changes. Note that actuation under the ULS load case does not affect the operational energy for adaptation which is computed under the SLS load case.

Table 5
Operational energy minimization.

$\min_{\mathbf{x}}$	$E_{operational}$	
s. t.	$\mathbf{K}\mathbf{u}^{L\_C\|SLS}_{jk}=\mathbf{P}^{L\|SLS}_{jk}$	$\forall j,\forall k\geqslant k^*$
	$\mathbf{F}^{L\_C\|SLS}_{jk}=\tilde{\mathbf{K}}\left(\mathbf{B}^{\mathrm{T}}\mathbf{u}^{L\_C\|SLS}_{jk}-\Delta\mathbf{L}^{L\|SLS}_{jk}\right)$	$\forall j,\forall k\geqslant k^*$
	$-\sigma^{C}\boldsymbol{\alpha}\leqslant\mathbf{F}^{P\_C\|SLS}+\mathbf{F}^{L\_C\|SLS}_{jk}\leqslant\sigma^{T}\boldsymbol{\alpha}$	$\forall j,\forall k\geqslant k^*$
	$-\mathbf{F}^{B}\leqslant\mathbf{F}^{P\_C\|SLS}+\mathbf{F}^{L\_C\|SLS}_{jk}$	$\forall j,\forall k\geqslant k^*$
	$-\mathbf{u}^{SLS}\leqslant\mathbf{u}^{L\_C\|SLS\|cdof}_{jk}\leqslant\mathbf{u}^{SLS}$	$\forall j,\forall k\geqslant k^*$
	$-\Delta L_{\text{limit}}\leqslant\Delta\mathbf{L}^{P}+\Delta\mathbf{L}^{L\|SLS}_{jk}\leqslant\Delta L_{\text{limit}}$	$\forall j,\forall k\geqslant k^*$
	$\Delta\mathbf{L}^{L\|SLS}_{jk}(m)=0$	$m\in I$
	$W^{F(1)}_{ijk}\leqslant\left(F^{P\_C\|SLS}_{i}+F^{L\|SLS}_{ijk}\right)\Delta L^{L\|SLS}_{ijk}$	$\forall i,\forall j,\forall k\geqslant k^*$
	$W^{\Delta F(1)}_{ijk}\leqslant\frac{1}{2}\Delta F^{L\|SLS}_{ijk}\Delta L^{L\|SLS}_{ijk}$	$\forall i,\forall j,\forall k\geqslant k^*$
	$W^{F(2)}_{ijk}\leqslant\left(F^{P\_C\|SLS}_{i}+\Delta F^{L\|SLS}_{ijk}\right)\left(-\Delta L^{L\|SLS}_{ijk}\right)$	$\forall i,\forall j,\forall k\geqslant k^*$
	$W^{\Delta F(2)}_{ijk}\leqslant\frac{1}{2}\left(-\Delta F^{L\|SLS}_{ijk}\right)\left(-\Delta L^{L\|SLS}_{ijk}\right)$	$\forall i,\forall j,\forall k\geqslant k^*$
	$W^{F(1)}_{ijk}\leqslant 0$	$\forall i,\forall j,\forall k\geqslant k^*$
	$W^{\Delta F(1)}_{ijk}\leqslant 0$	$\forall i,\forall j,\forall k\geqslant k^*$
	$W^{F(2)}_{ijk}\leqslant 0$	$\forall i,\forall j,\forall k\geqslant k^*$
	$W^{\Delta F(2)}_{ijk}\leqslant 0$	$\forall i,\forall j,\forall k\geqslant k^*$

4. Numerical examples

The TEO-MINLP formulation is applied to the design of a vertical cantilever truss and a simply-supported truss. The solutions produced by the TEO-MINLP method are compared with those produced by the TEO-Nested method. In the following, 'AS-MINLP' and 'AS-Nested' will be used to denote the solutions obtained by the two methods.

All structural elements are assumed to have a cylindrical hollow section and to be made of structural steel (S355) with a Young's modulus of 210 GPa, a density of 7800 kg/m^3 and an energy intensity of 36.5 MJ/kg [39]. To limit optimization complexity, the wall thickness of the element cross-section is set to 10% of the external radius and the minimum radius is set to 50 mm.

Table 6
Force and shape control with fail-safe constraints.

$\min_{\mathbf{x}}$	$\sum_i \left(\left\|\Delta\mathbf{L}_i^{P\|ULS}\right\| + \left\|\Delta\mathbf{L}_i^{L\|ULS}\right\|\right)$		
s.t.	$\mathbf{K}\mathbf{u}_j^{P\_C\|ULS} = \mathbf{P}_j^{P\|ULS}$	$\forall j$	
	$\mathbf{K}\mathbf{u}_j^{L\_C\|ULS} = \mathbf{P}_j^{L\|ULS}$	$\forall j$	
	$\mathbf{F}_j^{P\_C\|ULS} = \widetilde{\mathbf{K}}\left(\mathbf{B}^{\mathrm{T}}\mathbf{u}_j^{P\_C\|ULS} - \Delta\mathbf{L}_j^{P\|ULS}\right)$	$\forall j$	
	$\mathbf{F}_j^{L\_C\|ULS} = \widetilde{\mathbf{K}}\left(\mathbf{B}^{\mathrm{T}}\mathbf{u}_j^{L\_C\|ULS} - \Delta\mathbf{L}_j^{L\|ULS}\right)$	$\forall j$	
	$-\sigma^C\boldsymbol{\alpha} \leqslant \mathbf{F}_j^{P\_C\|ULS} \leqslant \sigma^T\boldsymbol{\alpha}$	$\forall j$	
	$-\sigma^C\boldsymbol{\alpha} \leqslant \mathbf{F}_j^{P\_C\|ULS} + \mathbf{F}_j^{L\_C\|ULS} \leqslant \sigma^T\boldsymbol{\alpha}$	$\forall j$	
	$-\mathbf{F}^B \leqslant \mathbf{F}_j^{P\_C\|ULS}$	$\forall j$	
	$-\mathbf{F}^B \leqslant \mathbf{F}_j^{P\_C\|ULS} + \mathbf{F}_j^{L\_C\|ULS}$	$\forall j$	
	$-\sigma^C\boldsymbol{\alpha} \leqslant \mathbf{F}_j^{P\_C\|ULS} + \mathbf{F}_j^{L\|ULS} \leqslant \sigma^T\boldsymbol{\alpha}$	$\forall j$	Fail-safe constraint
	$-\mathbf{F}^B \leqslant \mathbf{F}_j^{P\_C\|ULS} + \mathbf{F}_j^{L\|ULS}$	$\forall j$	
	$-\mathbf{u}^{SLS0} \leqslant \mathbf{u}_j^{P\_C\|ULS\|cdof} \leqslant \mathbf{u}^{SLS0}$	$\forall j$	
	$-\mathbf{u}^{SLS} \leqslant \mathbf{u}_j^{P\_C\|ULS\|cdof} + \mathbf{u}_j^{L\_C\|ULS\|cdof} \leqslant \mathbf{u}^{SLS}$	$\forall j$	
	$-\Delta L_{\text{limit}} \leqslant \Delta\mathbf{L}_j^{P\|ULS} \leqslant \Delta L_{\text{limit}}$	$\forall j$	
	$-\Delta L_{\text{limit}} \leqslant \Delta\mathbf{L}_j^{P\|ULS} + \Delta\mathbf{L}_j^{L\|ULS} \leqslant \Delta L_{\text{limit}}$	$\forall j$	
	$\Delta\mathbf{L}_j^{P\|ULS}(m) = 0$	$m \in I$	
	$\Delta\mathbf{L}_j^{L\|ULS}(m) = 0$	$m \in I$	
	$\Delta\mathbf{L}_i^{P\|ULS} = \Delta\mathbf{L}_j^{P\|ULS}$	if $\delta_i = \delta_j$	

The live load probability distribution is modelled using a log-normal distribution as described in Section 2.3. The service life is set to 50 years. The number of bins to sample the load probability distribution has a significant effect with regard to problem size for the TEO-MINLP process. In this case the number of variables increases drastically as the number of bins increases. Referring to Table 4 and Eq. (30), for each bin, $2n^p n^e$ variables related to element forces, $2n^p n^{fdof}$ to nodal displacements, $n^p n^e$ to actuator length changes, and $4n^p n^e$ to auxiliary variables must be added for a total of $n^p(7n^e + 2n^{fdof})$ variables per bin. To keep optimization feasible within a reasonable time, the live load probability distribution is discretized in 10 bins.

For the TEO-Nested process, the number of actuators n^{act} is set to the sum of the degree of static indeterminacy plus the number of controlled degrees of freedom (*cdof*). This is the minimum number of actuators that is required to control exactly the displacements of all *cdofs* [27]. For the TEO-MINLP process, the number of actuators can vary between an upper and a lower bound (Eq. (22)). In the following case studies, the upper bound $n^{\text{act}}_{\max}$ is set to the same number as that for the TEO-Nested process. The lower bound $n^{\text{act}}_{\min}$ can be set to any arbitrary value lower than $n^{\text{act}}_{\max}$. However, in order to reduce the size of the feasible solution space, the lower bound is set to $n^{\text{act}}_{\min} = n^{\text{act}}_{\max} - 2$. The maximum actuation length change is set to 500 mm. The actuator embodied energy is added to the structure embodied energy. For simplicity, it is assumed that the actuator mass is a linear function of the maximum required force capacity with a proportional constant of 0.1 kg/kN [40]. It is also assumed that an actuator is entirely made of steel with an energy intensity of 36.5 MJ/kg and a mechanical efficiency of 0.8 [41].

The indices *MUT* and UT_B denote utilization (demand over capacity) in terms of stress and stability:

$$MUT = \max\left(\frac{F_i}{F_i^S}\right) \tag{31}$$

$$UT_B = \max\left(\frac{F_i}{F_i^B}\right) \tag{32}$$

where F_i is the axial force in the i^{th} element, F_i^S is the force at which the element stress equals the admissible value for tension σ^T or compression σ^C and F_i^B is the critical buckling load. The material utilization factor *MUT* was introduced in [27] as an optimization variable. Note that for the TEO-MINLP process, the *MUT* is obtained through analysis. If the *MUT* is larger than 1.0, it means that there exists at least one element which is overstressed. Similarly, if UT_B is larger than 1.0, it means that there exists at least one element whose axial force exceeds the buckling load.

The index UT_{SLS} denotes the ratio between the maximum displacement among the controlled nodes (*cdofs*) and the *SLS* displacement limit:

$$UT_{SLS} = \max\left(\frac{u_i}{u_i^{SLS}}\right) \tag{33}$$

where u_i and u_i^{SLS} are the displacement and the serviceability limit for the i^{th} *cdof*, respectively. This index can be thought of as a control measure for the displacements. If UT_{SLS} is larger than 1.0, it means that there exists at least one nodal displacement that exceeds the serviceability limit.

Both TEO-MINLP and TEO-Nested formulations have been implemented in Matlab through own software. The main dependency for the TEO-MINLP process is the branch-and-bound algorithm implemented in Knitro [42] while for the TEO-Nested process the main dependency is the Sequential Quadratic Programming (SQP) algorithm built-in Matlab. The TEO-MINLP was solved on a NEOS Server [43] with a 2x Intel Xeon E5-2698 @ 2.30 GHz CPU and 192 GB RAM. The TEO-Nested was solved on a 2x Intel Xeon Silver 4116 @ 2.10 GHz CPU with 64 GB RAM. In addition, parallelization with 4 cores is employed to run the TEO-MINLP algorithm but no parallelization is implemented for the TEO-Nested algorithm.

4.1. Simply-supported truss

Two simply-supported planar trusses of 50 m span and 2.5 m depth, one statically determinate and one statically indeterminate, are considered in this case study. The serviceability limit is set to span/500 for all *cdofs*.

4.1.1. Statically determinate case

Fig. 4(a) shows dimensions and loading for the statically determinate simply-supported truss. Fig. 4(b) shows element numbering and the *cdofs* which are indicated by circles. The vertical displacement of all the top chord nodes and the horizontal displacement of the roller support are controlled for a total of 6 *cdofs*. For this reason, the number of actuators n^{act} for the TEO-Nested process is set to 6 and so is $n^{\text{act}}_{\max}$ for the TEO-MINLP process.

It is assumed that that this truss is part of a roof system. The dead load on the roof panels (out of plane) is set to 2.94 kN/m^2 (300 kg/m^2) resulting in a uniformly distributed load of 29.4 kN/m applied to the top chord of the truss. Two types of live load are considered: a wind load modelled as a negative pressure (L1) on the top chord of the truss and a lateral load L2. Both live loads have the same intensity of the dead load (live-to-dead load ratio is 1). The design loads and combination cases are summarized in Table 7.

Fig. 5(a) and (b) show the optimal adaptive structures AS-MINLP and AS-Nested obtained from the TEO-MINLP and TEO-Nested formulations, respectively. The element diameter is represented by line thickness – the thicker the line the bigger the diameter. The element cross-section area is indicated by color shading – a darker grey shade indicates a larger area. Fig. 5(c) is the weight-optimized passive structure which has been obtained through the optimization method described in [27]. The actuators are represented as integrated in the structure by replacing part of its ele-

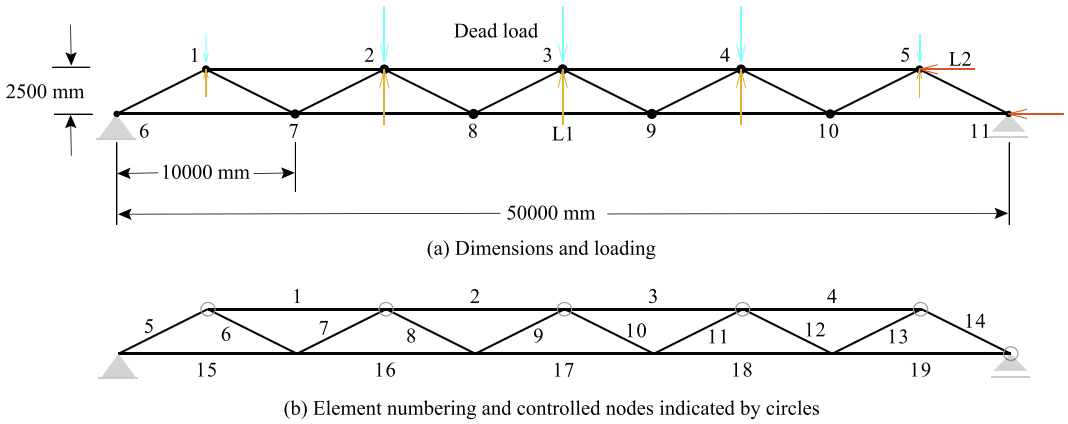

(a) Dimensions and loading

(b) Element numbering and controlled nodes indicated by circles

Fig. 4. Statically determinate simply supported truss.

Table 7
Load combination cases.

Case	Load factor	Permanent load	Load factor	Live load
LC1	1.35	dead load + self	1.5	–
LC2	0.9	dead load + self	1.5	L1 = 2.94 kN/m^2
LC3	1.35	dead load + self	1.5	L2 = 2.94 kN/m^2
LC4	0.9	dead load + self	1.5	L3 = L1 + L2

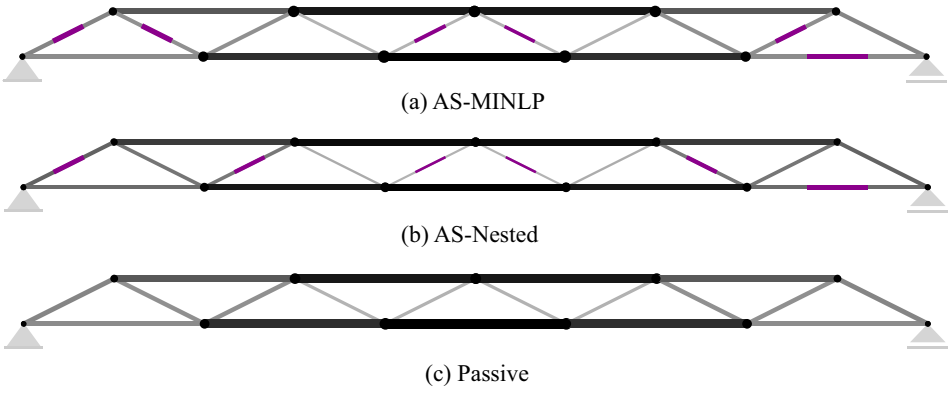

(a) AS-MINLP

(b) AS-Nested

(c) Passive

Fig. 5. Optimum solutions (a) AS-MINLP, (b) AS-Nested and (c) passive.

ments. Both AS-Nested and AS-MINLP have 6 actuators, but the layout is marginally different. Fig. 6 compares the bar chart of the element cross-section areas of the two adaptive solutions with that of the weight-optimized passive structure. Compared with the passive structure, all element cross-section areas of the AS-Nested and AS-MINLP are smaller. Some cross-section areas of the AS-MINLP (2, 3, 6, 7, 8, 9, 10, 11, 12, 13, 17, 18) are larger than those of the AS-Nested.

Fig. 7(a) shows the plot of the embodied, operational and total energy as a function of the *MUT* for the TEO-Nested process. The

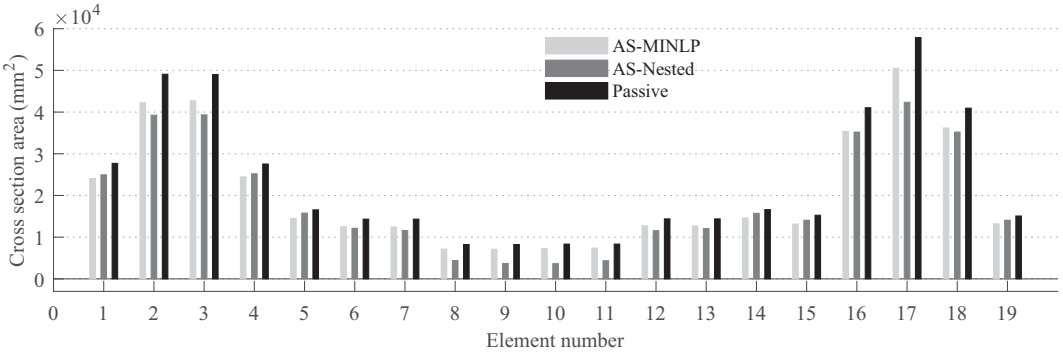

Fig. 6. Element cross-section areas.

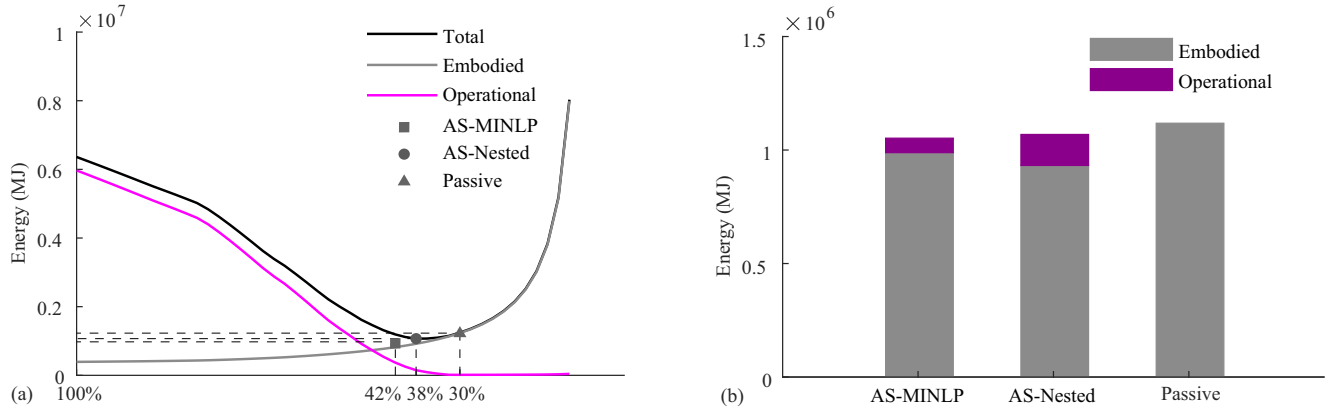

Fig. 7. (a) Embodied, operational and total energy vs *MUT*; (b) energy comparison.

minimum energy solution is obtained at an *MUT* of 38% for the TEO-Nested method. For comparison, the passive and the AS-MINLP solutions are indicated on the plot with a triangle and a square symbol respectively. The *MUT* for the AS-MINLP is 42% and that for the passive solution is 30% thus showing that material is better utilized in the AS-MINLP as well as the AS-Nested. As expected, the AS-MINLP configuration is not on the total energy curve of the TEO-Nested process. The AS-MINLP is a better configuration with respect to the AS-Nested one in total energy terms. However, the two solutions differ only marginally. Fig. 7(b) compares the embodied energy of the weight-optimized passive structure with the total energy of the two adaptive solutions. Mass and energy savings are 16.64% and 4.43% for the AS-Nested while 11.59% and 5.89% for the AS-MINLP. Table 8 gives further detail regarding embodied and operational energy of the two adaptive solutions.

Table 8 also gives the computation time required by TEO-Nested and TEO-MINLP. Regarding the TEO-MINLP computation time, two values are reported. The first value is the real time it took to obtain the optimal solution using parallelization with 4 cores while the second value is the CPU time (sum of the time used by each core). The CPU time is an approximate measure of the total time required when parallelization is not employed [44]. As expected, the computation time required by the TEO-MINLP is much larger than that required by the TEO-Nested method even though the former was ran on a better performing hardware and using parallelization. In this case the time required to obtain the AS-Nested is 1.26% of that required to obtain the AS-MINLP.

Fig. 8 shows the plot of the live load CDF indicating with a dotted line the load activation threshold (*LAT*). For load cases LC2 and LC4, the activation thresholds of the AS-Nested and AS-MINLP are both 2.61 kN/m^2. For LC3, actuation is not needed in both cases and therefore the *LAT* line is set to zero. The actuation time for both AS-Nested and AS-MINLP is 0.46 years.

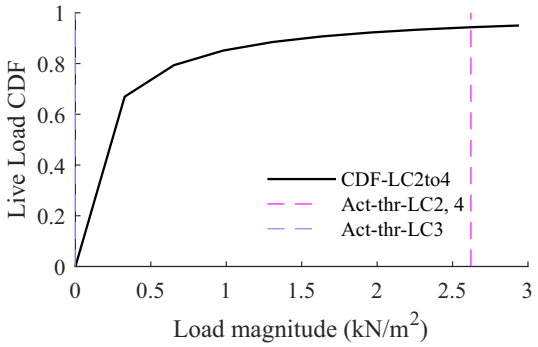

Fig. 8. Live load CDF and load activation threshold for AS-Nested and AS-MINLP.

Fig. 9 shows the bar chart for *MUT*, UT_B and UT_{SLS} before and after control. *MUT* and UT_B are always smaller than 1.0 which means that the element forces are always lower than the admissible value (admissible stress) and critical load, hence fail-safe conditions are satisfied. In this case, *MUT* and UT_B do not change before and after control. This is because the structure is statically determinate and therefore the actuator length changes do not modify the internal forces but only the node positions (small strains assumption). As expected, serviceability limit is not respected when the structure is not controlled i.e. UT_{SLS} is larger than 1.0. However, after control, UT_{SLS} is smaller than1.0 for both cases.

For further comparison, optimization metrics of the adaptive solution obtained through the TEO-Nested process but accounting only for one-phase adaptation are also listed in Table 8. Both embodied energy and operational energy are much smaller than those obtained considering a two-phase adaptation. The activation threshold is smaller, which results in a much longer actuation time (2.54 years). The operational energy required in the second phase

Table 8
Summary of results.

	MUT	Embodied energy (MJ)	Operational energy (MJ)	Mass savings	Energy savings	Actuation threshold (LC4)	Actuation time (years)	Computation time (seconds)
AS-MINLP	0.42	1.00×10^6	0.06×10^6	11.59%	5.89%	2.61 kN/m^2	0.46	4061.63 (16205.31)
AS-Nested (2 phase)	0.38	0.93×10^6	0.14×10^6	16.64%	4.43%	2.61 kN/m^2	0.46	51.63
AS-Nested (1 phase)	1.00	0.40×10^6	0.002×10^6	63.93%	63.74%	1.31 kN/m^2	2.54	40.03
Passive	0.30	1.12×10^6	0	–	–	–	–	0.46

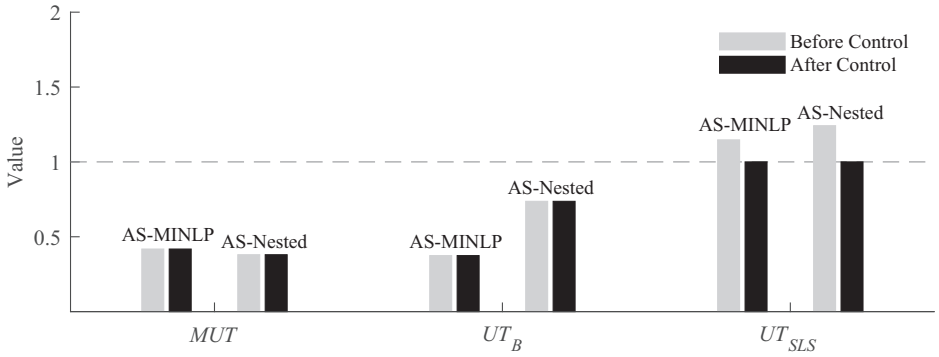

Fig. 9. Utilization factors *MUT*, UT_B and UT_{SLS}.

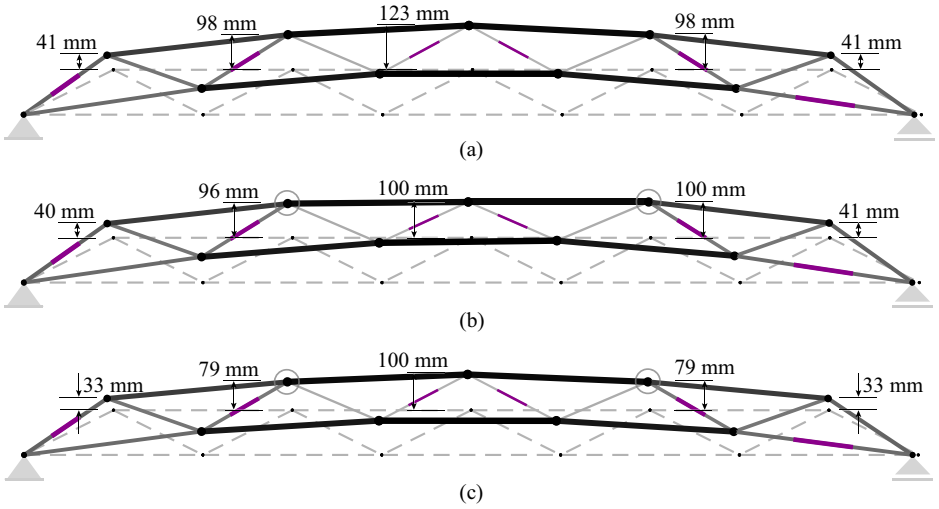

Fig. 10. Deformed and controlled shape under LC2: (a) AS-Nested before control, (b) AS-Nested after control, (c) AS-Nested after control (smooth control), deformation magnification ×20.

of the adaptation process is not negligible for this configuration. In this case, when two-phase adaptation is considered, the optimal solution has to be much stiffer (higher embodied energy) in order to minimize the total energy. Because the live load is opposite to the dead load, most of the energy is required to control the structure into the optimal state under permanent load after the live load is removed (second phase).

Fig. 10(a) shows the deformed shape of the AS-Nested before control under load case LC2. Fig. 10(b) shows that the controlled shapes have a significant curvature change at the nodes indicated by circles. This effect is caused by assigning the same displacement limit u^{SLS} to all *cdofs*. A better way to to set u^{SLS} is to consider the curvature rate of change between consecutive bays in order to avoid kinks through shape control.

Fig. 10(c) shows the shape controlled to have a smooth change of curvature between consecutive bays. Shape control with curvature constraints usually requires more operational energy than shape control without curvature constraints. In this case, smooth shape control causes an increase of 26.75% in total energy.

In order to investigate the influence of the structure span-to-depth ratio (S/D) on mass and energy savings, two other cases with the same span but a S/D ratio of 30 and 40 are carried out. Fig. 11 shows the bar chart of mass and energy savings. As expected, the savings increase as the S/D ratio increases because the design becomes more stiffness governed reaching a maximum of 25.50% in mass terms and 15.96% in energy terms for the TEO-MINLP solution. For S/D ratios of 30 and 40, the TEO-Nested method produces marginally better solutions than the TEO-MINLP method.

4.1.2. Statically indeterminate case

Fig. 12(a) shows dimensions and loading for the statically indeterminate simply-supported truss, which are the same as those for the determinate case. Fig. 12(b) shows element numbering and the *cdofs* which are indicated by circles. The vertical displacement of all the top chord nodes except the end nodes and the horizontal displacement of the roller support are controlled for a total of 5 *cdofs*. Since the degree of static indeterminacy r is 5, the number of actuators n^{act} for the TEO-Nested process is set to 10 and so is n^{act}_{max} for the TEO-MINLP process.

The AS-MINLP and AS-Nested are shown in Fig. 13(a) and (b) respectively. For comparison, the weight-optimized passive structure is shown in Fig. 13(c). Element dimeters and cross-section areas are indicated by line thickness variation and color shading as described in Section 4.1.1. Different to the AS-Nested which has 10 actuators, the AS-MINLP was obtained with only 8 actuators. The actuator layout of the AS-MINLP is substantially different to that of the AS-Nested. Fig. 14 compares the bar chart of the element cross-section areas for the two adaptive solutions with that of the weight-optimized passive structure. With respect to the determinate case, the cross-section distribution in the indeterminate truss is more uneven. Regarding the AS-Nested, the biggest

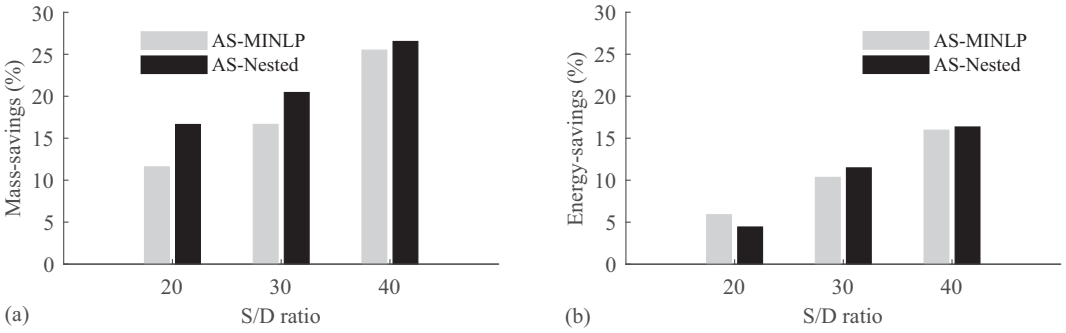

Fig. 11. Mass (a) and energy (b) savings for different span-to-depth (S/D) ratios.

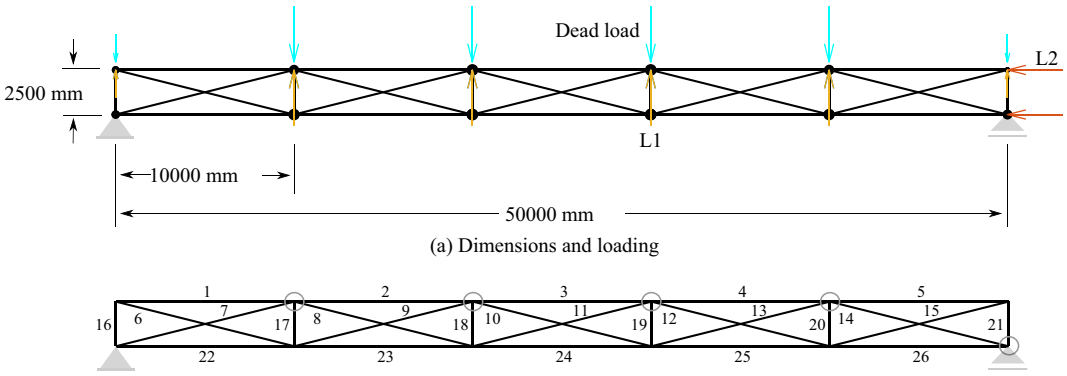

Fig. 12. Statically indeterminate simply supported truss.

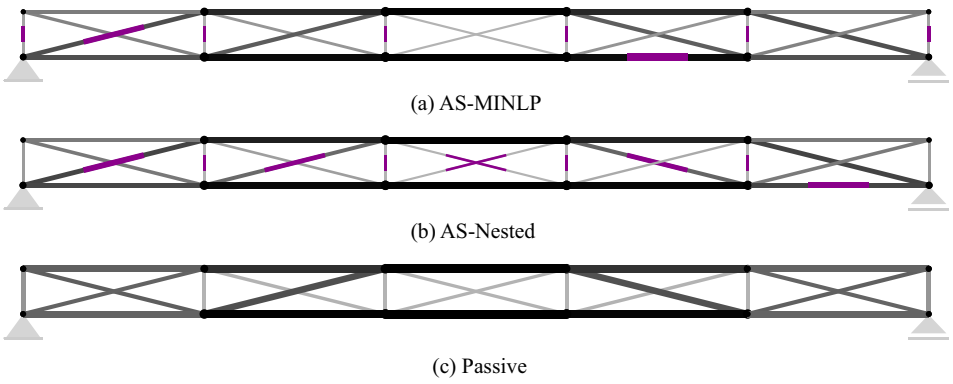

Fig. 13. Optimum solutions (a) AS-MINLP, (b) AS-Nested and (c) passive.

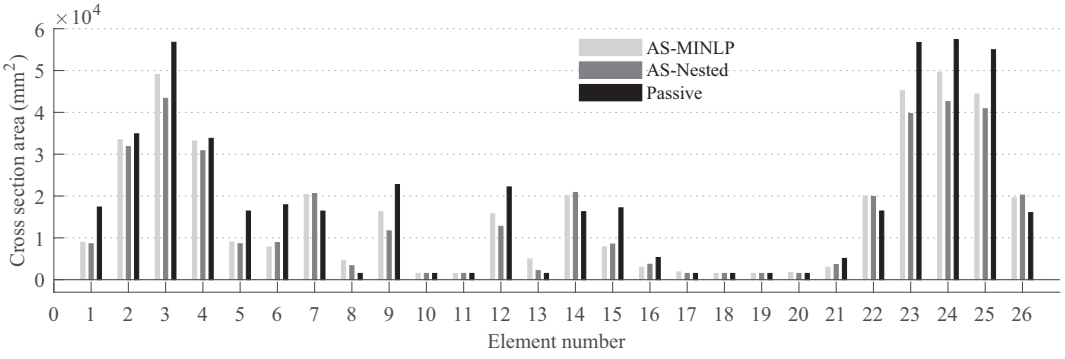

Fig. 14. Element cross-section areas.

and smallest diameter are 540 mm and 100 mm for element 3 and elements 10, 11, 17, 18, 19, and 20 respectively. Regarding the AS-MINLP, the biggest and smallest diameter are 577 mm and 100 mm for element 24 and elements 10, 11, 18, and 19 respectively.

Fig. 15(a) shows the plot of the embodied, operational and total energy as a function of the *MUT* for the TEO-Nested process. The minimum energy solution is obtained at an *MUT* of 38% for the TEO-Nested method and at an *MUT* of 43% for the TEO-MINLP method. The *MUT* for the passive solution is 30% thus showing that material is much better utilized in the AS-MINLP as well as the AS-Nested. As for the determinate case, the two adaptive solutions differ only marginally. Fig. 15(b) compares the embodied energy of the weight-optimized passive structure with the total energy of the two adaptive solutions. Mass and energy savings are 19.85% and 0.22% for the AS-Nested while 11.17% and 5.39% for the AS-MINLP solution. Table 9 gives further detail regarding embodied and operational energy of the two adaptive solutions. The computation time required by the TEO-Nested is 1.89% of that required by the TEO-MINLP process (Table 9).

Fig. 16 shows the plot of the live load CDF indicating with a dotted line the *LAT*. For load cases LC2 and LC4, the activation thresholds of the AS-Nested and AS-MINLP are both 2.61 kN/m^2. As for the determinate case, adaptation is not needed for LC3. The actuation time for both AS-Nested and AS-MINLP is 0.46 years.

Fig. 17 shows the bar chart for *MUT*, UT_B and UT_{SLS} before and after control. *MUT* and UT_B are always smaller than or equal to 1.0 before and after control, hence fail-safe conditions are satisfied. In addition, for both solutions, after control the *MUT* reduces to the values indicated in Table 9 (control states). Deflection limits are not respected when the structure is not controlled i.e. UT_{SLS} is larger than 1.0. However, after control, UT_{SLS} reduces to 1.0 for both cases.

Similar to the determinate case, the solution produced by the TEO-Nested formulation using one-phase adaptation (Table 9) gives much higher mass and energy savings because the operational energy required by the second phase of the adaptation process is not accounted for. This result confirms that for simply supported trusses subjected to a live load opposite to the permanent load, the operational energy required by the second phase actuation cannot be ignored.

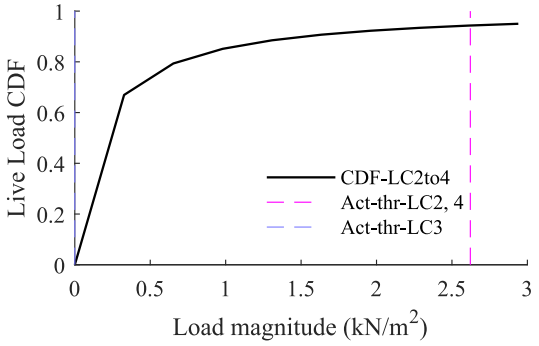

Fig. 16. Live load CDF and load activation threshold for AS-Nested and AS-MINLP.

Shape control with curvature constraints (Fig. 18(c)) can be achieved at the cost of 31.13% energy increase compared to shape control without curvature constraints (Fig. 18(b)).

In order to investigate the influence of the structure span-to-depth ratio (S/D) on mass and energy savings, two other cases with the same span but a S/D ratio of 30 and 40 are carried out. Fig. 19 shows the bar chart of mass and energy savings. As expected, the savings increase as the S/D ratio increases reaching a maximum of 32.09% in mass terms and 20.09% in energy terms for the TEO-MINLP solution . The TEO-MINLP produces better solutions than the TEO-Nested process for all cases.

4.2. Cantilever truss

Two cantilever trusses of 100 m height and 12.5 m width, one statically determinate and one statically indeterminate, are consid-

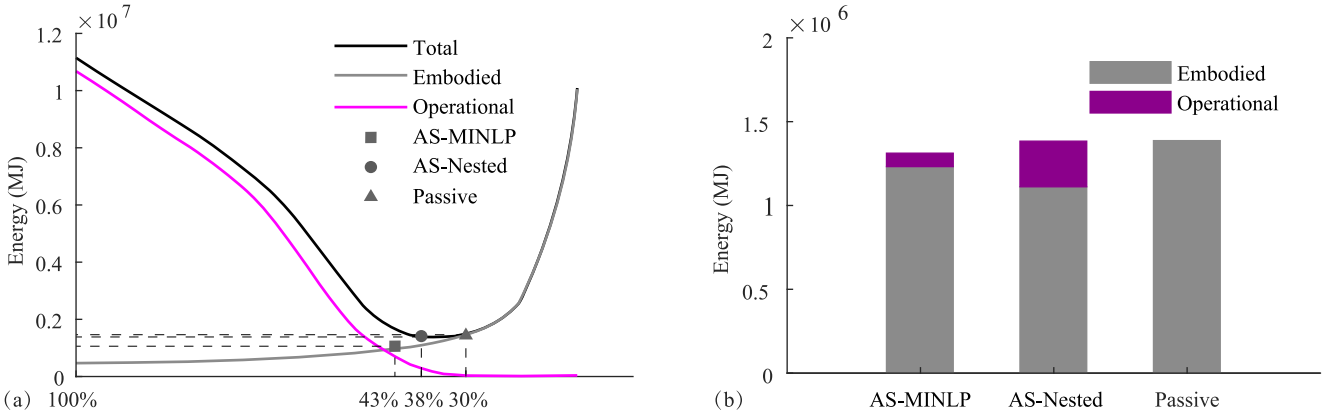

Fig. 15. (a) Embodied, operational and total energy vs *MUT*; (b) energy comparison.

Table 9
Summary of results.

	MUT	Embodied energy (MJ)	Operational energy (MJ)	Mass-savings	Energy-savings	Actuation threshold (LC4)	Actuation time (years)	Computation time (seconds)
AS-MINLP	0.43	1.23×10^6	0.08×10^6	11.17%	5.39%	2.61 kN/m^2	0.46	9828.13 (28678.50)
AS-Nested (2 phase)	0.38	1.11×10^6	0.27×10^6	19.85%	0.22%	2.61 kN/m^2	0.46	186.03
AS-Nested (1 phase)	0.85	0.53×10^6	0.20×10^6	61.82%	47.23%	0.98 kN/m^2	3.72	228.17
Passive	0.30	1.39×10^6	0	–	–	–	–	1.05

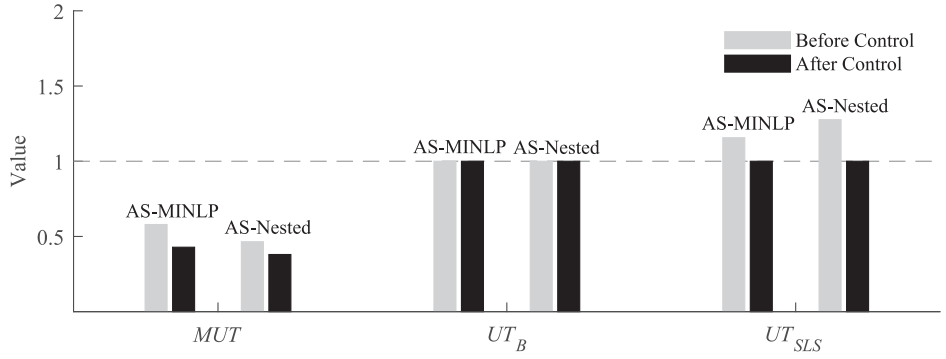

Fig. 17. Utilization factors *MUT*, UT_B and UT_{SLS}.

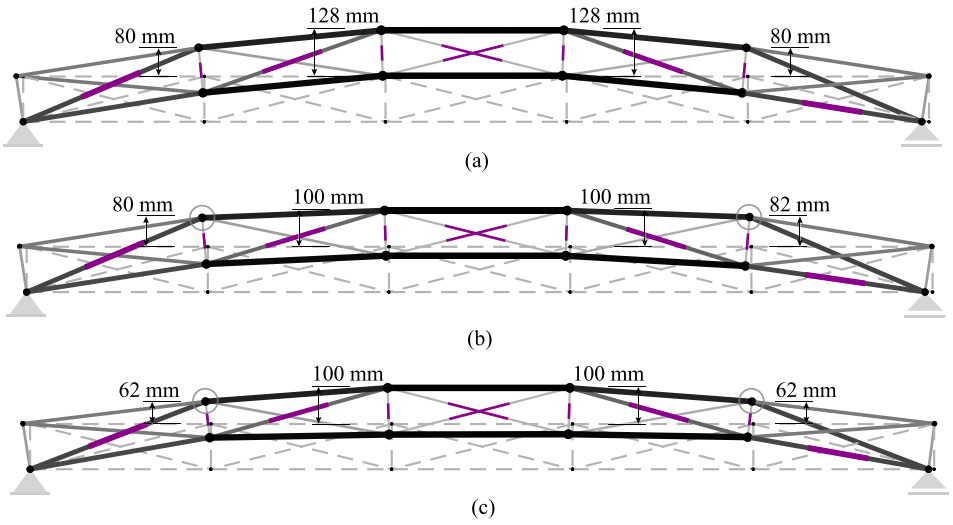

Fig. 18. Deformed and controlled shape under LC2: (a) AS-Nested before control, (b) AS-Nested after control, (c) AS-Nested after control (smooth control), deformation magnification ×20.

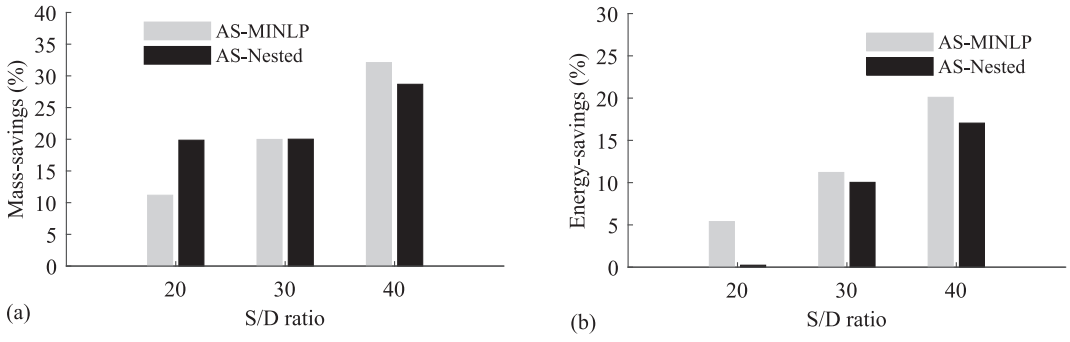

Fig. 19. Mass (a) and energy (b) savings for different span-to-depth (S/D) ratios.

ered in this case study. The serviceability limit is set to height/500 for all *cdofs*.

4.2.1. Statically determinate case

Fig. 20(a) shows dimensions and loading for the statically determinate cantilever truss. Fig. 20(b) shows element numbering and the *cdofs* which are indicated by circles. The horizontal displacement of all unconstrained nodes is controlled for a total of 16 *cdofs*. The number of actuators n^{act} for the TEO-Nested process is set to 16 and so is n^{act}_{max} for the TEO-MINLP process.

It is assumed that this truss is the primary structure of a multi-story building reduced to two dimensions. The dead load is set to 2.94 kN/m^2 (300 kg/m^2) resulting in a uniformly distributed load of 36.75 kN/m applied every 4 m for each floor. Three load cases are considered: one is self-weight + dead load (vertical); the other two are horizontally distributed loads in opposite directions whose intensity varies with the square root of the height to approximate a wind-type (live) load (L1 and L2). The live-load maximum intensity is set to 2.94 kN/m^2 (live-to-dead load ratio of 1). Table 10 summarizes all load cases.

The AS-MINLP and AS-Nested are shown in Fig. 20(c) and (d), respectively. For comparison, the weight-optimized passive structure is shown in Fig. 20(e). Element diameters and cross-section areas are indicated by line thickness variation and color shading

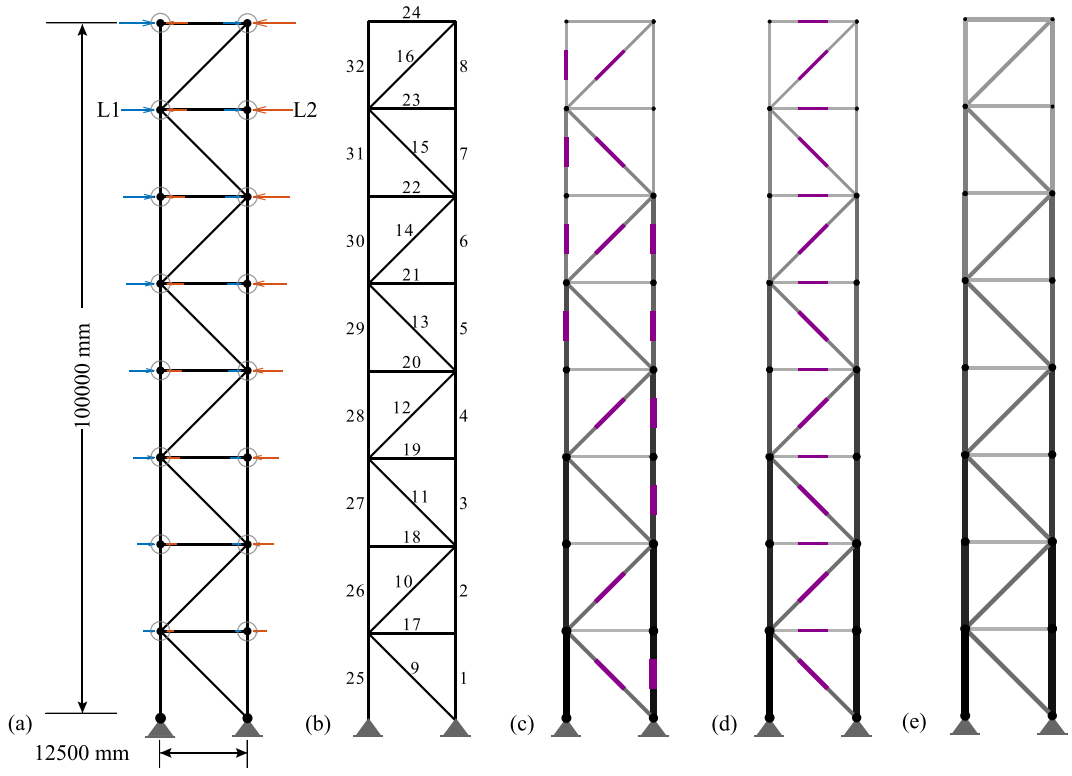

Fig. 20. Statically determinate cantilever truss: (a) dimensions and loading; (b) element numbering and *cdofs*, (c) AS-MINLP, (d) AS-Nested, (e) passive.

Table 10
Load combination cases.

Case	Load factor	Permanent load	Load factor	Live load
LC1	1.35	dead load + self-weight	1.5	–
LC2 and LC3	1.35	dead load + self-weight	1.5	2.94 kN/m^2

as described in Section 4.1.1. Different to the AS-Nested which has 16 actuators, the AS-MINLP was obtained with 15 actuators. For the AS-Nested, the actuators are placed on diagonal and horizontal elements. For the AS-MINLP some actuators are placed on the vertical elements. Fig. 21 compares the bar chart of the element cross-section areas for the two adaptive solutions with that of the weight-optimized passive structure. The cross-section area distribution of the AS-Nested and AS-MINLP are similar. On average, the element cross-section areas of the adaptive designs are 40% smaller than those in the passive design.

Fig. 22(a) shows the plot of the embodied, operational and total energy as a function of the *MUT* for the TEO-Nested process. The minimum energy solution is obtained at an *MUT* of 34% for TEO-Nested and 43% for TEO-MINLP. The *MUT* for the passive solution is 20% thus showing that material is better utilized in the AS-MINLP as well as AS-Nested. As for the simply-supported case, the two adaptive solutions differ only marginally. Fig. 22 (b) compares the embodied energy of the weight-optimized passive structure with the total energy of the two adaptive solutions. Mass and energy savings are 34.48% and 20.99% for the AS-Nested

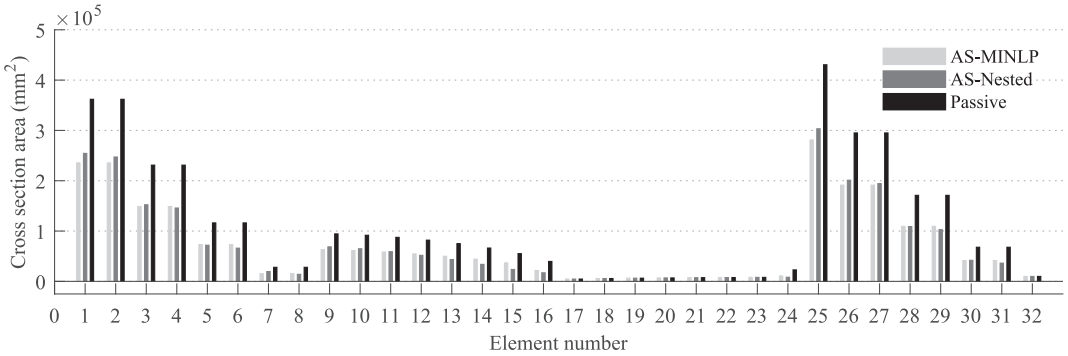

Fig. 21. Element cross-section areas.

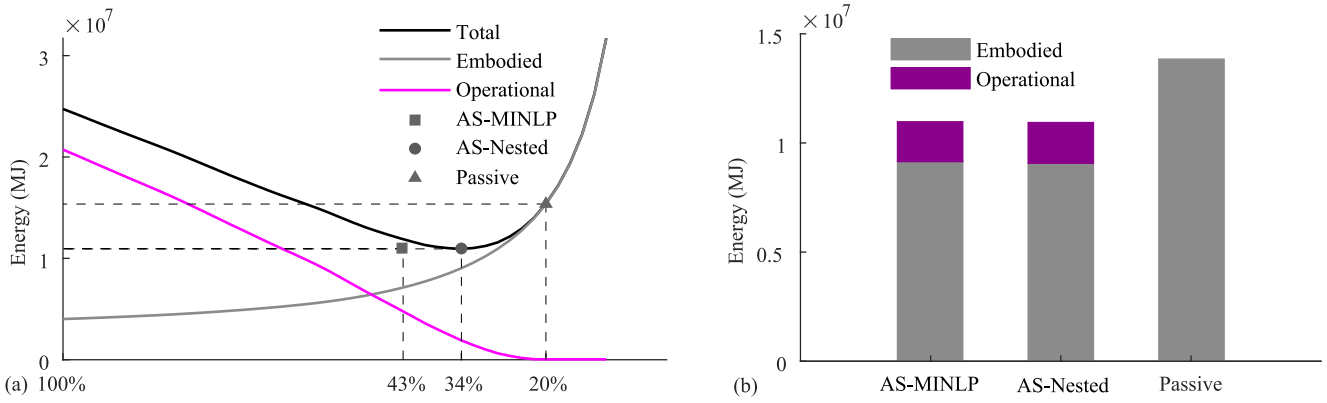

Fig. 22. (a) Embodied, operational and total energy vs *MUT*; (b) energy comparison.

while 33.94% and 20.75% for the AS-MINLP. Table 11 gives further detail regarding embodied and operational energy of the two solutions. The computation time required by the TEO-Nested process is 3.42% of that required by the TEO-MINLP process (Table 11). In this case, the solution produced by the TEO-Nested formulation using one-phase adaptation is identical to that produced by considering a two-phase adaptation. Different to the simply-supported case very little operational energy is needed for the second phase of the adaptation process (see Section 2.2).

Fig. 23 shows the plot of the live load CDF indicating with a dotted line the *LAT*. Both AS-Nested and AS-MINLP have the same activation threshold at 1.96 kN/m^2 and a combined actuation time of 1.80 years for LC2 and LC3.

Fig. 24 shows the bar chart for *MUT*, UT_B and UT_{SLS} before and after control. *MUT* and UT_B are always smaller than or equal to 1.0 before and after control, hence fail-safe conditions are satisfied. Without control, UT_{SLS} is bigger than 1 for both solutions – the maximum displacement is above the deflection limit of 200 mm. UT_{SLS} reduces to 1 through control for both solutions.

Fig. 25(b) shows that the controlled shapes have a drastic curvature change at the nodes indicated by circles. This effect is caused by assigning the same displacement limit u^{SLS} to all *cdofs*. Fig. 25(c) shows the shape controlled to have a smooth change of curvature between consecutive bays. In this case, smooth shape control causes an increase of 26.62% in total energy.

In order to investigate the influence of height-to-depth ratio (H/D) on mass and energy-savings, two other cases with the same height but a H/D ratio of 12 and 16 are carried out. Fig. 26 shows the bar chart of mass and energy savings. As expected, the savings increase as the H/D ratio increases reaching a maximum of 44.82% in mass terms and 34.59% in energy terms for the TEO-MINLP solution. The TEO-Nested produces marginally better solutions than the TEO-MINLP for all cases.

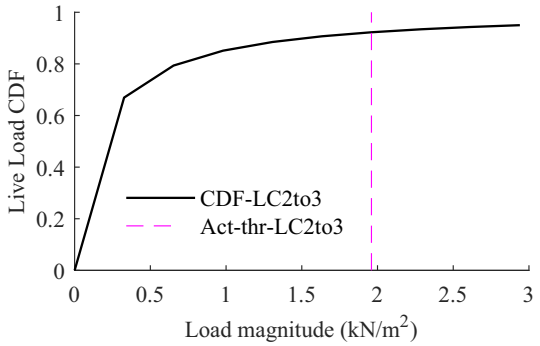

Fig. 23. Live load CDF and load activation threshold for AS-Nested and AS-MINLP.

4.3. Statically indeterminate case

Fig. 27(a) shows dimensions and loading for the statically indeterminate cantilever truss, which are the same as those for the determinate case. Fig. 27(b) shows element numbering and the *cdofs* which are indicated by circles. The horizontal displacements of all unconstrained nodes are controlled for a total of 16 *cdofs*. Since the degree of static indeterminacy *r* is 8, the number of actuators n^{act} for the TEO-Nested process is set to 24 and so is n^{act}_{max} for the TEO-MINLP process.

The AS-MINLP and AS-Nested are shown in Fig. 27(c) and (d) respectively. For comparison, the weight-optimized passive structure is shown in Fig. 27(e). Element dimeters and cross-section areas are indicated by line thickness variation and color shading as described in Section 4.1.1. Both AS-Nested and AS-MINLP have 24 actuators. In the AS-MINLP some actuators are placed on the vertical element while in the AS-Nested all actuators are placed on the diagonal bracers and horizontal elements. Fig. 28 compares

Table 11
Summary of results.

	MUT	Embodied energy (MJ)	Operational energy (MJ)	Mass-savings	Energy-savings	Actuation threshold (LC2-LC3)	Actuation time (years)	Computation time (seconds)
AS-MINLP	0.43	0.91×10^7	0.18×10^7	33.94%	20.75%	1.96 kN/m^2	1.80	2107.45 (8244.43)
AS-Nested (2 phase)	0.34	0.91×10^7	0.19×10^7	34.48%	20.99%	1.96 kN/m^2	1.80	72.10
AS-Nested (1 phase)	0.34	0.91×10^7	0.19×10^7	34.48%	20.99%	1.96 kN/m^2	1.80	62.61
Passive	0.20	1.38×10^7	0	–	–	–	–	1.23

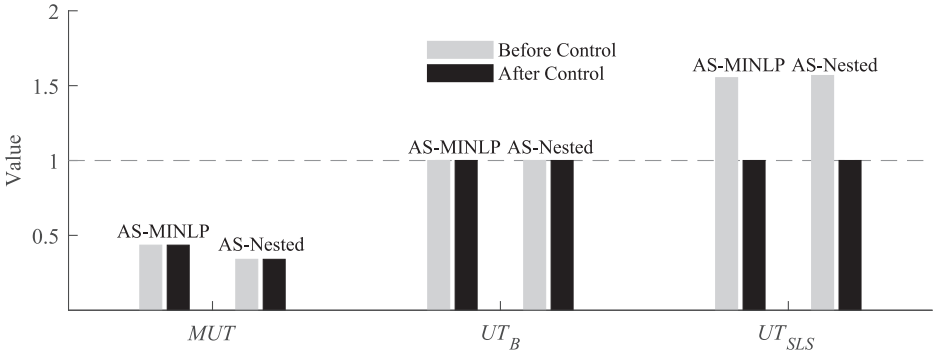

Fig. 24. Utilization factors *MUT*, UT_B and UT_{SLS}.

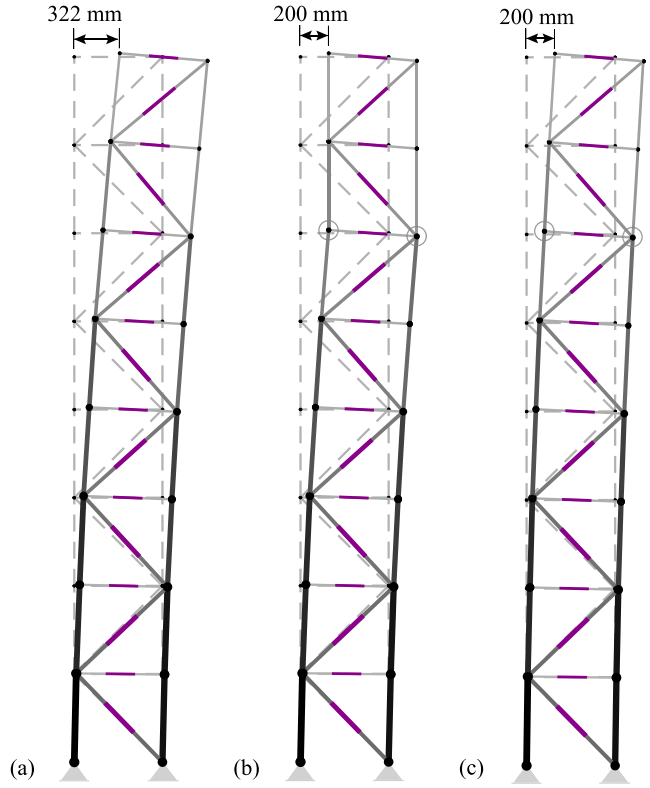

Fig. 25. Deformed and controlled shape under LC2: (a) AS-Nested before control, (b) AS-Nested after control, (c) AS-Nested after control (smooth control), deformation magnification ×20.

the bar chart of the cross-section areas of the two adaptive designs with that of the equivalent weight-optimized passive design. Most elements of the AS-MINLP have a smaller cross-section (approximately 10% smaller on average) than those of the AS-Nested.

Fig. 29 (a) shows the plot of the embodied, operational and total energy as a function of the *MUT* for the TEO-Nested process. The minimum energy solution is obtained at an *MUT* of 30% for TEO-Nested and 36% for TEO-MINLP. The *MUT* for the passive solution is 22% thus showing that material is better utilized in the AS-MINLP as well as AS-Nested. As for the determinate case, the two adaptive solutions differ only marginally. Fig. 29(b) compares the embodied energy of the weight-optimized passive structure with the total energy of the two adaptive solutions. Mass and energy savings are 24.08% and 16.62% for the AS-Nested while 31.54% and 20.47% for the AS-MINLP. Table 12 gives further detail regarding embodied and operational energy of the two solutions. The computation time required by the TEO-Nested process is 14.52% of that required by the TEO-MINLP (Table 12).

There is a relatively substantial difference (4.6%) in energy savings terms between the solution produced by the TEO-Nested formulation using one-phase adaptation to that produced by considering two-phase adaptation. This indicates the operational energy required by the second phase of the adaptation process cannot be neglected for this case.

Fig. 30 shows the plot of the live load CDF indicating with a dotted line the *LAT*. Both AS-Nested and AS-MINLP have the same activation threshold of 2.29 kN/m^2 and a combined actuation time of 1.17 years for LC2 and LC3.

Fig. 31 shows the bar chart for *MUT*, UT_B and UT_{SLS} before and after control. *MUT* and UT_B are always smaller than or equal to 1.0 before and after control, hence fail-safe conditions are met. In addition, for both solutions, after control the *MUT* reduces to the

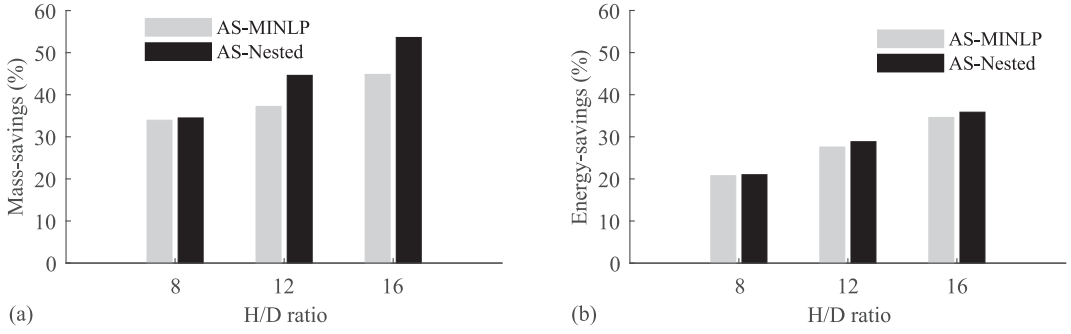

Fig. 26. Mass (a) and energy (b) savings for different height-to-depth (H/D) ratios.

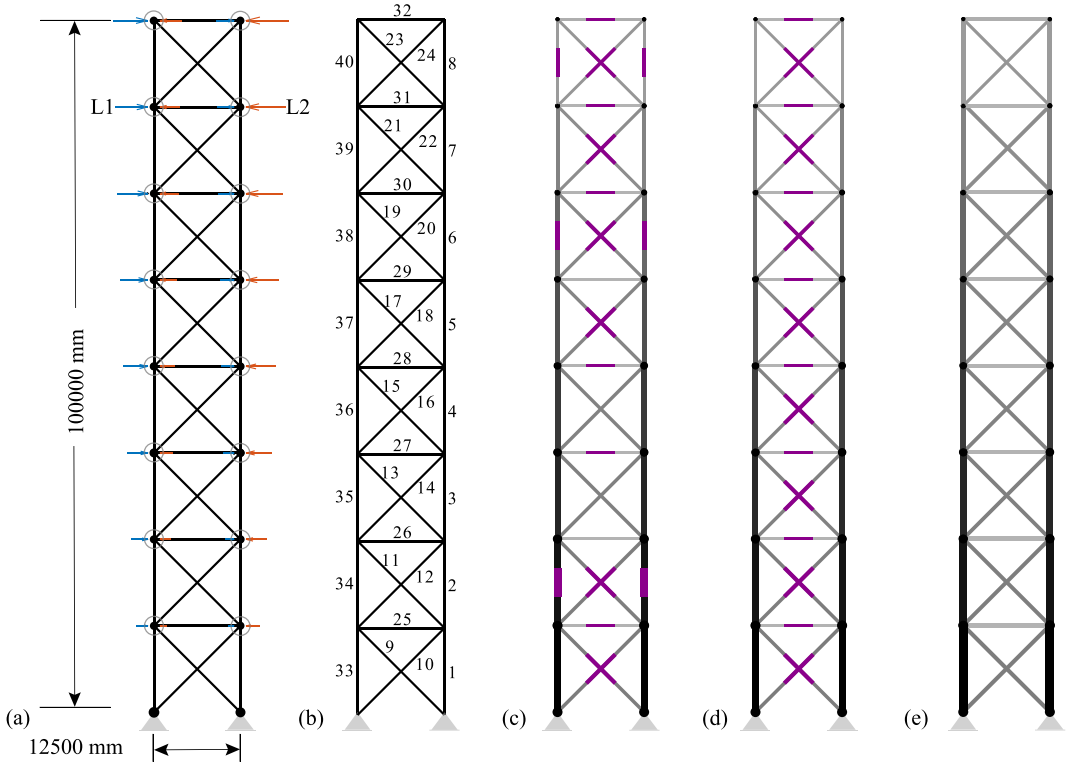

Fig. 27. Indeterminate cantilever truss: (a) dimensions and loading, (b) element numbering and *cdofs*, (c) AS-MINLP, (d) AS-Nested, (e) passive.

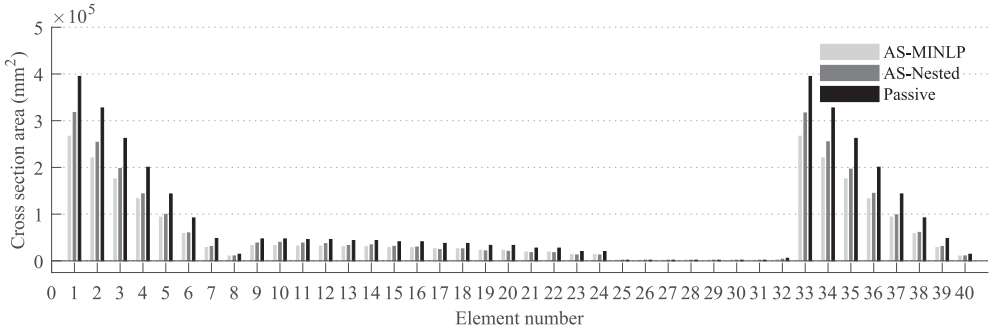

Fig. 28. Element cross-section areas.

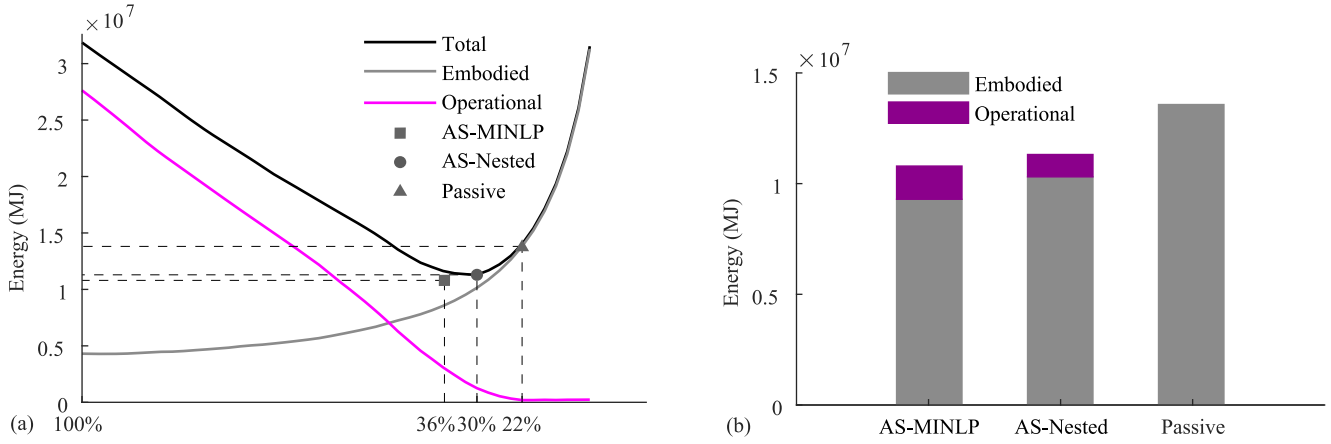

Fig. 29. (a) Embodied, operational and total energy vs *MUT*; (b) energy comparison.

Table 12
Summary of results.

	MUT	Embodied energy (MJ)	Operational energy (MJ)	Mass-savings	Energy-savings	Actuation threshold (LC4)	Actuation time (years)	Computation time (seconds)
AS-MINLP	0.36	0.93×10^7	0.15×10^7	31.54%	20.47%	2.29 kN/m^2	1.17	2582.62 (9877.13)
AS-Nested (2 phase)	0.30	1.02×10^7	0.11×10^7	24.08%	16.62%	2.29 kN/m^2	1.17	375.52
AS-Nested (1 phase)	0.33	0.94×10^7	0.13×10^7	30.62%	21.20%	2.29 kN/m^2	1.17	263.48
Passive	0.22	1.35×10^7	0	–	–	–	–	2.17

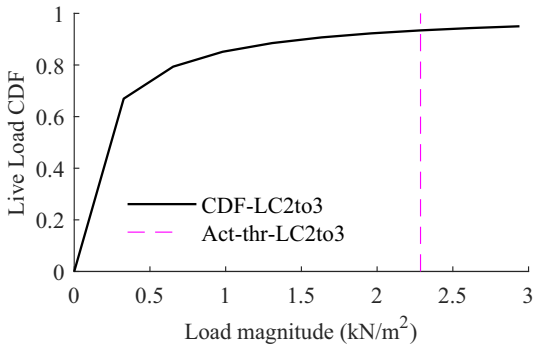

Fig. 30. Live load CDFs and activation thresholds for AS-Nested and AS-MINLP.

values indicated in Table 12 (optimal states). Without control, UT_{SLS} is bigger than 1 for both solutions – the maximum displacement is above the deflection limit of 200 mm. UT_{SLS} reduces to 1.0 through control.

Similar to the determinate case, shape control with curvature constraints (Fig. 32(c)) can be achieved at the cost of 11.8% energy increase compared to shape control without curvature constraints (Fig. 32(b)).

In order to investigate the influence of height-to-depth ratio (H/D) on mass and energy-savings, two other cases with the same height but a H/D ratio of 12 and 16 are carried out. Fig. 33 shows the bar chart of mass and energy savings. As expected, the savings increase as the S/D ratio increases reaching a maximum of 44.59% in mass terms and 34.29% in energy terms for the solution produced by the TEO-MINLP. For H/D ratios of 8 and 12, the TEO-MINLP method produces better designs in energy terms compared to the TEO-Nested method. Opposite is the case for a H/D ratio of 16.

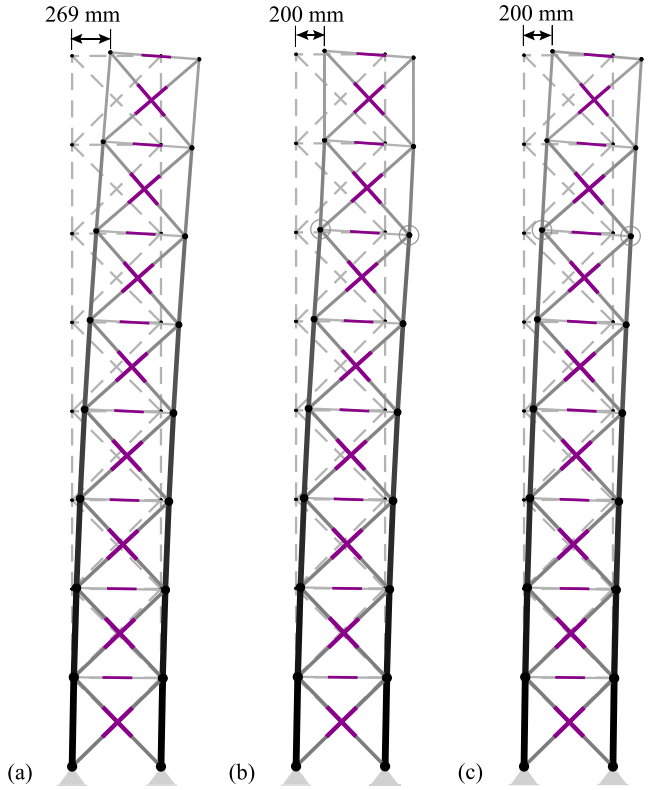

Fig. 32. Deformed and controlled shape under LC2: (a) AS-Nested before control, (b) AS-Nested after control, (c) AS-Nested after control (smooth control),deformation magnification ×20.

5. Discussion

This paper gives a new All-In-One implementation (TEO-MINLP) of an existing formulation (TEO-Nested) [27] for the synthesis of minimum energy adaptive structures. The formulation has been implemented for reticular structures equipped with linear actuators. The new implementation is based on Mixed Integer Non-Linear Programming. Element cross-section, element forces, nodal displacements and actuator commands are treated as continuous design variables while the actuator locations as binary design

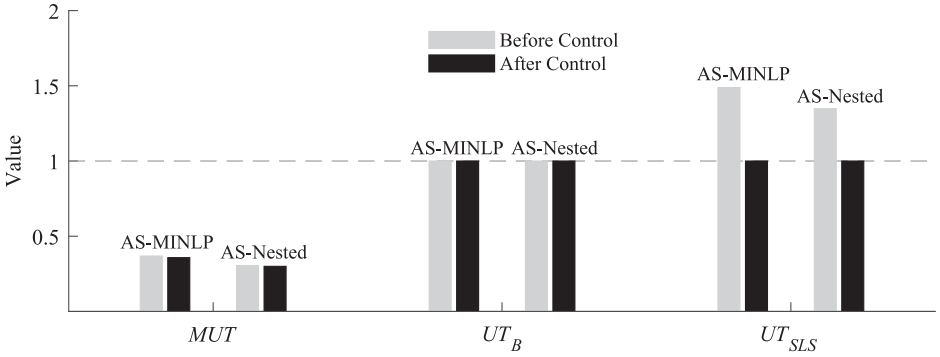

Fig. 31. Utilization factors *MUT*, UT_B and UT_{SLS}.

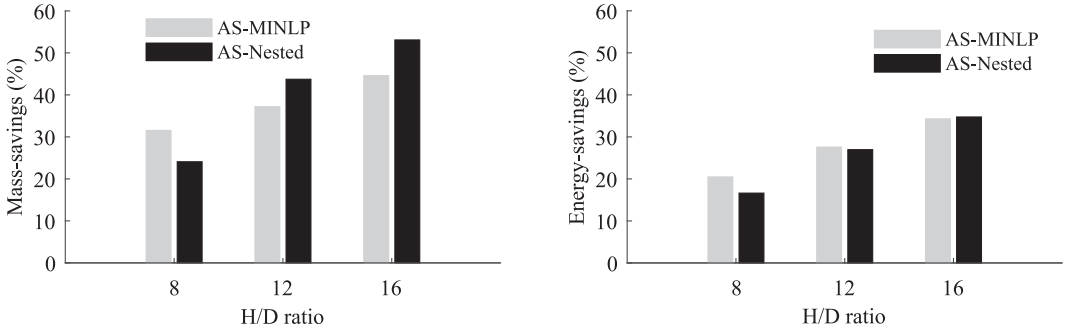

Fig. 33. Mass (a) and energy (b) savings for different height-to-depth (H/D) ratios.

variables. The objective is to minimize the structure whole-life energy which comprises the energy embodied in the material and the operational part for structural adaptation during service. For all the cases studied in this paper, the TEO-MINLP method has produced either marginally better or practically identical configurations in energy saving terms than the solutions obtained through the TEO-Nested method. This result proves that even though the nested approach does not use a direct way to solve the All-in-One problem, it is able to produce solutions which are similar to the optimal ones. Note that the solution obtained through the MINLP formulation is a local optimum because the model is non-convex.

On the other hand, the computational efficiency of the two approaches are very different. For the four cases studied in this paper, the computation time required by the TEO-MINLP are much larger than those required by the TEO-Nested model. On average, the computation time required by TEO-Nested is only 5.72% of that required by TEO-MINLP. Actuator layout optimization involves assigning a certain number of actuators to a set of available sites, which makes the search space to grow factorially with the number of structural elements. For this reason, the MINLP-based approach is often impractical for structures made of a large number of elements.

Although fail-safe constraints have not been directly included in the main optimization model, fail-safe conditions have been verified through a post-analysis process. Since the examples studied in this work are stiffness governed design problems, the governing constraint is the serviceability limit on deflections and therefore the optimization model has been simplified by excluding fail-safe constraints. However, as explained in Section 3.2.7, the inclusion of the fail-safe constraints expressed through Eq. (19) is a straightforward addition to the main model. For a practical application of either the TEO-Nested or TEO-MINLP formulation, suitable fail-safe criteria should be considered which depend on the reliability of the control system. The reader is referred to [27] for a further discussion on fail-safe conditions for adaptive structures.

Identical assumptions have been taken for both methods to carry out a rigorous benchmark. A relatively coarse discretization of the load probability distribution function has been employed to reduce the computation time required by TEO-MINLP. Using a finer discretization only increases the scale but it does not affect the nature of the optimization problem (e.g. non-linearity and non-convexity). Therefore, the conclusions reached in this work do not depend on the discretization of the load probability distribution function.

6. Conclusion

This work has successfully proven numerically that the TEO-Nested formulation [27] produces similar solutions to the optima obtained through the TEO-MINLP formulation. In addition, it has also been proven that the TEO-Nested is significantly more efficient in computation time terms and thus it is more suitable to be employed for large-scale design problems.

Results have shown that the TEO-MINLP method tends to perform better than the TEO-Nested method for the design of statically indeterminate structures. With the assumption of small deformations, the effect of actuation is a simultaneous change of the internal forces and node positions for statically indeterminate configurations but no change of internal forces occurs in statically determinate configurations. For this reason, the design problem (objective function and constrains) has a stronger non-linearity in the case of statically indeterminate structures, which can be handled in a more stable manner by the All-In-One formulation implemented for the TEO-MINLP method. For this reason, the TEO-MINLP formulation should be used to design statically indeterminate adaptive structures for small or medium scale problems depending on computational resources.

The two phase adaptation process considered in this study produces more accurate results compared to the one phase adaptation process considered in [27]. The second phase is required to control the structure into the optimal shape under permanent load after the live load is removed. The energy required in the second phase might be negligible in some cases but in other cases (Section 4.1) it is significant.

It has been assumed that the energy required to fabricate and install joints and supports is identical for the passive and active solution and therefore it has not been included in the embodied energy computation. This is because the structure topology is identical for both structures and therefore an equal amount of joints and supports is required in both cases. This assumption is conservative because, generally, the passive solution requires bigger cross-sections and it is heavier than the adaptive solution, therefore energy requirements to supply joints and supports are likely to be higher for the passive case. Including consideration for the energy required by joints and supports could be a possible direction for future works.

The state-of-the-art branch and bound algorithm has been employed in this work. However, this method cannot produce solutions for large-scale design problems within a reasonable computation time. Future work could look into developing new algorithms (e. g. heuristic based) to improve the computational efficiency of the All-in-One model for large-scale design problems. Future work could also look into developing new methods to extend the current TEO formulation to geometry and topology optimization by adding node coordinates and element connectivity to the design variables.

7. Data reproduction

All data including source code is available upon request from the corresponding author. For up to date contact information visit http://www.gennarosenatore.com.

Acknowledgements

The authors thankfully acknowledge Swiss National Science Foundation who provided core funding for this research via project 200021_182033 (*Structural Adaptation through Large Shape Changes*).

References

[1] Soong TT, Chang JCH. Active vibration control of large flexible structures. Shock Vibr Inform Center Shock Vib Bull 1982;52.
[2] Soong TT. State-of-the-art review: active structural control in civil engineering. Eng Struct 1988;10(2):74–84.
[3] Utku S. Theory of adaptive structures: incorporating intelligence into engineered products. Routledge; 2018.
[4] Abdel-Rohman M, Leipholz HH. Active control of tall buildings. J Struct Eng 1983;109(3):628–45.
[5] Reinhorn AM, Soong TT, Lin RC, Riley MA, Wang YP, Aizawa S., et al., Active bracing system: a full-scale implementation of active control. National Center for Earthquake Engineering Research. 14 Aug. 1992. Buffalo. US.; 1992.
[6] Rodellar J, Mañosa V, Monroy C. An active tendon control scheme for cable-stayed bridges with model uncertainties and seismic excitation. J Struct Control 2002;9(1):75–94.
[7] Xu B, Wu ZS, Yokoyama K. Neural networks for decentralized control of cable-stayed bridge. J Bridge Eng 2003;8(4):229–36.
[8] Tibert G. Deployable tensegrity structures for space applications. KTH; 2002.
[9] Fest E, Shea K, Domer B, Smith IFC. Adjustable tensegrity structures. J Struct Eng 2003;129(4):515–26.
[10] Veuve N, Safaei SD, Smith IFC. Deployment of a tensegrity footbridge. J Struct Eng 2015;141(11):4015021.
[11] Ali NBH, Smith IFC. Dynamic behavior and vibration control of a tensegrity structure. Int J Solids Struct 2010;47(9):1285–96.
[12] Santos FA, Rodrigues A, Micheletti A. Design and experimental testing of an adaptive shape-morphing tensegrity structure, with frequency self-tuning capabilities, using shape-memory alloys. Smart Mater Struct 2015;24 (10):105008.
[13] Kota S, Hetrick JA, Osborn R, Paul D, Pendleton E, Flick P, et al. Design and application of compliant mechanisms for morphing aircraft structures. Smart structures and materials 2003: industrial and commercial applications of smart structures technologies, 2003.
[14] Hasse A, Campanile LF. Design of compliant mechanisms with selective compliance. Smart Mater Struct 2009;18(11):115016.
[15] Previtali F, Ermanni P. Performance of a non-tapered 3D morphing wing with integrated compliant ribs. Smart Mater Struct 2012;21(5):55008.
[16] Lienhard J, Schleicher S, Poppinga S, Masselter T, Milwich M, Speck T, et al. Flectofin: a hingeless flapping mechanism inspired by nature. Bioinspiration Biomimetics 2011;6(4):45001.
[17] Soong T, Manolis G. Active structures. J Struct Eng 1987;113:2290–302.
[18] Smith MJ, Grigoriadis KM, Skelton RE. The optimal mix of passive and active control. 1991 American Control Conference, Boston, MA, 1991.
[19] Dhingra A, Lee BH. Multi-objective design of actively controlled structures using a hybrid optimization method. Int J Numer Meth Eng 1995;38:3383–401.
[20] Begg D, Liu X. On simultaneous optimization of smart structures - Part II: Algorithms and examples. Comput Methods Appl Mech Eng 2000;184:25–37.
[21] Teuffel P. "Entwerfen Adaptiver Strukturen [Doctoral dissertation]. Struttgart: University of Stuttgart - ILEK; 2004.
[22] Skelton R, Hanks B, Smith M. Structure redesign for improved dynamic response. J Guid Control Dyn 1992;15(5):1271–8.
[23] Khot NS. Multicriteria optimization for design of structures with active control. J Aerosp Eng 1998;11(2):45–51.
[24] Cimellaro G, Soong T, Reinhorn A. Optimal integrated design of controlled structures. The 14th world conference on earthquake engineering, Beijing, 2008.
[25] Molter A, da Silveira OAA, Bottega V, Fonseca JSO. Integrated topology optimization and optimal control for vibration suppression in structural design. Struct Multidiscip Optim 2013;47(3):389–97.
[26] Senatore G, Duffour P, Hanna S, Labbe F, Winslow P. Adaptive structures for whole life energy savings. Int Assoc Shell Spatial Struct (IASS) 2011;52 (4):233–40. December n. 170.
[27] Senatore G, Duffour P, Winslow P. Synthesis of minimum energy adaptive structures. Struct Multidiscip Optim 2019;60(3):849–77.
[28] Senatore G, Duffour P, Winslow P. Energy and cost analysis of adaptive structures: case studies. J Struct Eng (ASCE) 2018;144(8):04018107.
[29] Senatore G, Duffour P, Winslow P. Exploring the application domain of adaptive structures. Eng Struct 2018;167:608–28.
[30] Senatore G, Duffour P, Winslow P, Wise C. Shape control and whole-life energy assessment of an "Infinitely Stiff" prototype adaptive structure. Smart Mater Struct 2018;27(1):015022.
[31] Reksowardojo AP, Senatore G, Smith IFC. Design of structures that adapt to loads through large shape changes. J Struct Eng (ASCE) 2019;146(5):04020068.
[32] Reksowardojo AP, Senatore G, Smith IFC. Experimental testing of a small-scale truss beam that adapts to loads through large shape changes. Front Built Environ 2019;5(93). https://doi.org/10.3389/fbuil.2019.00093.
[33] European Environment Agency. Material Resources and Waste - The European environment - State and outlook. Publications Office of the European Union, Luxembourg; 2010.
[34] International Energy Agency. "2018 Global Status Report," UN Environment Programme; 2018.
[35] Kaethner S, Burridge J. Embodied CO2 of structural frames. Struct Eng 2012;90 (5):33–40.
[36] Patnaik S. An integrated force method for discrete analysis. Int J Numer Meth Eng 1973;6(2):237–51.
[37] Patnaik SN, Hopkins DA, Halford GR. Integrated force method solution to indeterminate structural mechanics problems; 2004.
[38] Patnaik SN, Coroneos RM, Hopkins DA. Recent advances in the method of forces: integrated force method of structural analysis. Adv Eng Softw 1998;29 (3–6):463–74.
[39] Hammond GP, Jones CI. Embodied energy and carbon in construction materials. Proc Inst Civ Eng Energy 2008;161(2):87–98. https://doi.org/10.1680/ener.2008.161.2.87.
[40] ENERPAC. E328e Industrial Tools – Europe; 2016 [Online]. Available: https://www.enerpac.com/en-us/downloads.
[41] Huber JE, Fleck NA, Ashby MF. The selection of mechanical actuators based on performance indices. Proc Roy Soc A 1997;453(1965):2185–205.
[42] Nocedal J. Knitro: an integrated package for nonlinear optimization. In: Large-scale nonlinear optimization. Springer; 2006. p. 35–60.
[43] Czyzyk J, Mesnier MP, Moré JJ. The NEOS server. IEEE Comput Sci Eng 1998;5 (3):68–75.
[44] "Parallelism — Artelys Knitro 12.0 User's Manual," [Online]. Available: https://www.artelys.com/docs/knitro/2_userGuide/parallelism.html.
[45] Weidner S, Kelleter C, Sternberg P, Haase W, Geiger F, Burghardt T, et al. The implementation of adaptive elements into an experimental high-rise building. Steel Construction: Design and Research 2018;11(2):109–17.
[46] Sobek W. Ultra-lightweight construction. International Journal of Space Structures 2016;31(1):74–80.
[47] B. Frohlich, J. Wagner, M. Bohn, O. Sawdony and P. Eberhard, "Combining Optimal Control and Shape Optimization for an Adaptive Engineering Structure with Parameterized Reduced Order Finite Element Models," in *IX ECCOMAS Thematic Conference on Smart Structures and Materials SMART 2019*, Paris, 2019.
[48] Wagner JL, Gade J, Heidingsfeld M, Geiger F, von Scheven M, Böhm M, et al. On steady-state disturbance compensability for actuator placement in adaptive structures. Automatisierungstechnik 2018;66(8):591–603.
[49] M. Böhm, J. Wagner, S. Steffen, W. Sobek and O. Sawodny, "Homogenizability of Element Utilization in Adaptive Structures," in *15th International Conference on Automation Science and Engineering (CASE)*, Vancouver, 2019.